Article:
Hippler, M. orcid.org/0000-0002-3956-3922, Oeltjen, L. and Quack, M. orcid.org/0000-0002-1351-8584 (2023) Mode-selective vibrational-tunneling dynamics in the N=2 triad of the hydrogen-bonded (HF)2 cluster. Israel Journal of Chemistry, 63 (7-8). e202300092. ISSN 0021-2148

https://doi.org/10.1002/ijch.202300092

Research Article

Israel Journal of Chemistry
www.ijc.wiley-vch.de

doi.org/10.1002/ijch.202300092

Mode-Selective Vibrational-Tunneling Dynamics in the $N=2$ Triad of the Hydrogen-Bonded $(HF)_2$ Cluster

Michael Hippler,*[a, b] Lars Oeltjen,[a] and Martin Quack*[a]

Dedicated to Prof. Helmut Schwarz on the occasion of his 80th birthday.

Abstract: Rovibrationally resolved spectra of the $N_j=2_2$, $K_a=0\leftarrow1$ transition and of the $N_j=2_3$, $K_a=0\leftarrow0$ and $K_a=1\leftarrow0$ transitions of the hydrogen-bonded $(HF)_2$ have been measured in the near infrared range near 1.3 μm by cw-diode laser cavity ring-down spectroscopy in a pulsed supersonic slit jet expansion. The spectroscopic assignment and analysis provided an insight into the dynamics of these highly-excited vibrational states, in particular concerning the predissociation of the hydrogen bond and the tunneling process of the hydrogen bond switching. Together with our previously analyzed spectra of the $N_j=2_1$ and $N_j=2_2$ components, the mode-specific dynamics in all three components of this triad can now be compared. In the $N=2$ triad, the HF-stretching vibration is excited by two quanta with similar excitation energy, but the quanta are distributed in three different ways, which has a distinct influence on the dynamics. The observed band centers and tunneling splittings are in agreement with our recent calculations on the $(HF)_2$ potential energy hypersurface SO-3, resolving the long-standing discussion about the symmetry ordering of polyad levels in this overtone region. The results are also discussed in relation to the general questions of non-statistical reaction dynamics of polyatomic molecules and clusters and in relation to quasi-adiabatic channel above barrier tunneling.

1. Introduction

Much of chemical dynamics and kinetics is commonly understood with statistical theories such as transition state theory (TST) or the quasi-equilibrium theory (QET) of unimolecular fragmentation in mass spectra and related theories such as RRKM (Rice-Ramsperger-Kassel-Marcus) theory or the statistical adiabatic channel model (SACM). In these theories, which still govern the textbooks, it is assumed that fast intramolecular energy redistribution leads to a micro-canonical quasi-equilibrium state in polyatomic molecules on times scales of less than picoseconds, while subsequent reaction dynamics and kinetics can be calculated using the quasi-equilibrium state as a starting point. During the last decades a new understanding leads to the possibility that the intramolecular energy redistribution can be the rate limiting step, which results then in highly non-statistical or mode-selective reaction dynamics. A very early experimental example of this kind was reported in Ref. [1] for reactions of radical cations, which identifies Helmut Schwarz as one of the pioneers in the field of non-statistical reaction dynamics in polyatomic molecules and ions. As an example of quantitative early theoretical work on reaction dynamics involving the hypothesis of rate limiting intramolecular energy flow, see Ref. [2].

An interesting early experimental example where intramolecular energy flow is in fact inhibited quite strongly was provided by the dissociation of the hydrogen bonded HF dimer, a minicluster, after excitation of the HF stretching overtones at energies exceeding the dissociation energy of about 12.7 kJ mol^{-1} by a factor of more than seven, still showing quite structured spectra indicating long lifetimes for vibrational predissociation.[3,4] Hydrogen bonded systems are intermediate cases between strong covalent bonds with binding energies of about 100 kJ mol^{-1} and larger, and weakly bonded van der Waals molecules such as (rare gas-HF) complexes,[5] with binding energies of 1 to 3 kJ mol^{-1}, and simpler, very different dynamics. The current understanding of inhibited vibrational energy flow in (HFHF) systems is schematically shown in Figure 1.

The high frequency HF stretching vibrations can be adiabatically separated from the low frequency modes in the cluster which are lower by about a factor of ten in frequency. Thereby for each stretching vibrational level one obtains an effective vibrationally adiabatic potential hypersurface for the motion of the low frequency modes, where Figure 1 shows a section of this potential as a function of the hydrogen bond length as defined by the distance R_{AB} of the center of masses of the two HF monomers in the dimer. In the dimer, there are

[a] *M. Hippler, L. Oeltjen, M. Quack*
Physical Chemistry, ETH Zürich, CH-8093 Zürich, Switzerland
E-mail: M.Hippler@sheffield.ac.uk
Martin@Quack.ch
Homepage: www.ir.ethz.ch
[b] *M. Hippler*
Dept of Chemistry, University of Sheffield, Sheffield S3 7HF, England
Homepage: https://michaelhippler.sites.sheffield.ac.uk

Israel Journal of Chemistry

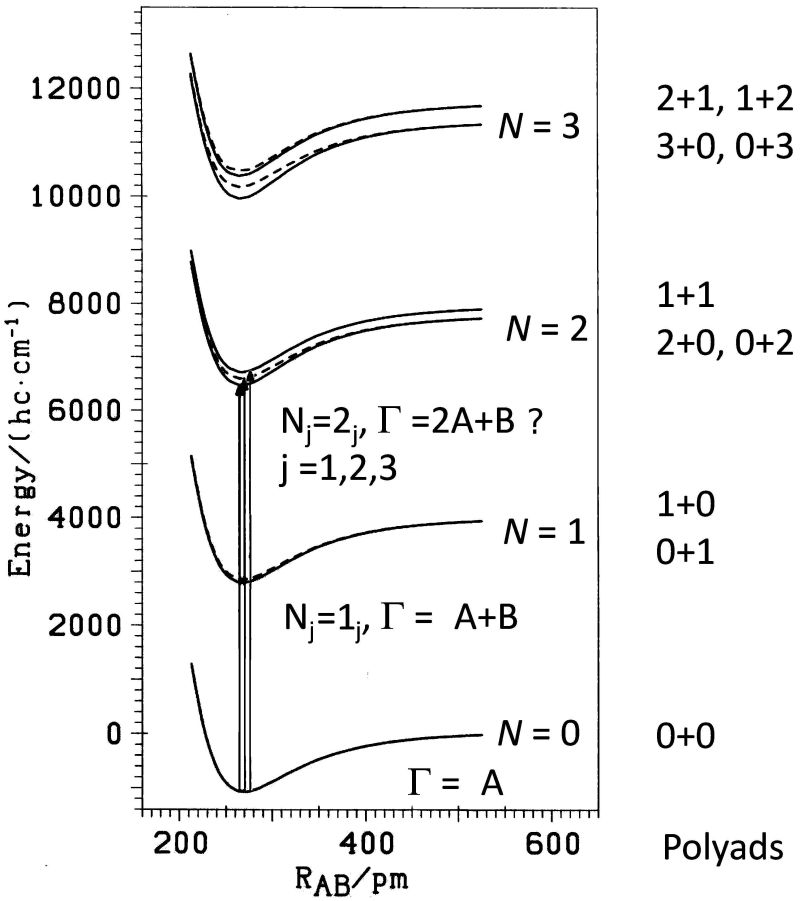

Figure 1. Quasi-adiabatic channel potentials for hydrogen bond dissociation in the HF dimer $(HF)_2$. The polyad quantum number N gives the total number of HF stretching quanta and the subscript j orders the sublevels of the polyad according to increasing energy. The various possible combinations of quanta in the donor and acceptor are given on the right hand side as $(v_{don} + v_{acc})$. R_{AB} is the center-of-mass distance of the two HF monomers in the dimer. The symmetry species Γ (symmetric A or antisymmetric B) in the polyads as predicted from simple models for $N=1$ and $N=2$ is indicated as well, where the question mark for $N=2$ indicates an open question being resolved here in opposition to the simple predictions. See main text in section 4 for more details, and also Refs. [3, 6].

two high frequency HF stretching modes of slightly different frequency, either in the hydrogen bond donor HF or in the hydrogen bond acceptor HF monomer. Therefore one has one such potential for zero quanta in the HF stretching modes, two potentials with one HF stretching quantum (either in the bonded or in the non-bonded, 'free' HF stretching mode, the classical normal modes correspond closely to such localized excitations, see Ref. [7]), three potentials for excitation with two quanta of HF stretching, and so on, depending on the number of possible combinations, as shown in Figure 1. These vibrationally quasi-adiabatic channel potentials support long-lived states with slow vibrational predissociation, qualitatively similar to the slow electronic predissociation which often arises because of the separation of electronic and nuclear motion following the Born-Oppenheimer (BO) approximation. The HF dimer can be considered to be the simplest prototypical case for such a dynamics in hydrogen bonded clusters.

A second prototypical process which occurs in such hydrogen-bonded clusters is the hydrogen bond rearrangement, which is illustrated by Figure 2. In this process, the 'bonded' and the 'free' hydrogen in the cluster exchange their role. The rearrangement can occur by tunneling through a low barrier of about 350 cm^{-1} as shown for the lowest channel with no HF stretching excitation in the lower part. Again, one can consider the process with, say, two quanta of HF stretching excitation, at energies exceeding the 'electronic tunneling barrier' by more than a factor of 20. The rearrangement high above the barrier would need no tunneling on the multidimensional BO-potential hypersurface. However, when one defines again a vibrationally quasi-adiabatic channel for the rearrangement, depending on the various HF stretching excitations, then one finds 'tunneling' through an effective potential barrier. This phenomenon which arises from inhibited vibrational energy flow due to quasi-adiabatic separation of modes, has been called 'quasi-adiabatic channel above barrier tunneling' and leads to tunneling spectra very similar to other cases of

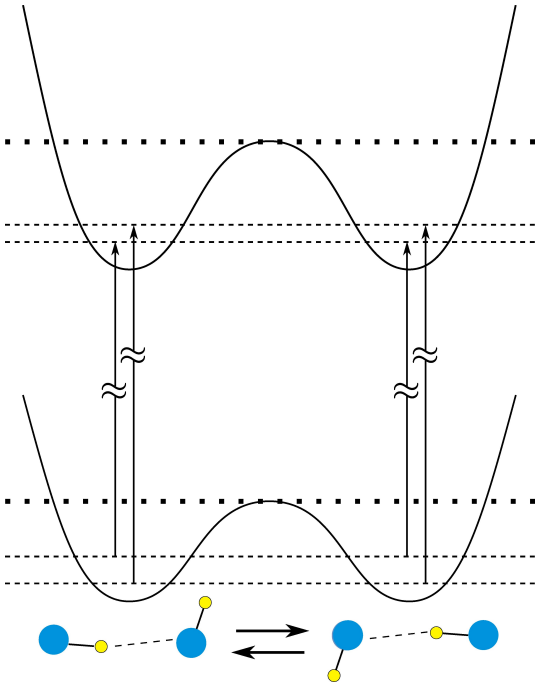

Figure 2. Scheme for hydrogen bond rearrangement tunneling in the HF dimer in the ground state and in an excited state with some HF stretching excitation (not to scale; see also Refs. [8, 9]).

tunneling.[10] These two processes, hydrogen bond dissociation and hydrogen bond rearrangement occur in hydrogen bonded clusters ubiquitously explaining the importance to achieve their understanding, from larger clusters to liquids.[11–13]

Indeed, hydrogen bonding and hydrogen-bonded aggregates are also of great importance in science and everyday life. Hydrogen bonds determine, for example, the structure and dynamics of liquids such as water, and they strongly influence DNA base pairing and protein folding.[14–17] Hydrogen bonding is thus one of the most relevant structural and dynamic elements in molecular aggregates. To achieve a better understanding of hydrogen bonding many different methods from spectroscopy to quantum chemical calculations have been applied to a large variety of hydrogen-bonded systems, but in general the analysis is rather difficult due to the complexity and number of molecules involved. Therefore, as already mentioned, the dimer (HFHF) has been chosen as a particularly simple prototypical system by spectroscopists and theoreticians.[3,4,6–8,10,18–40] In 1972 Dyke, Howard and Klemperer provided the rotationally resolved spectra of $(HF)_2$ using molecular beam electric resonance studies in the microwave region.[18] Subsequently, high-resolution spectroscopic investigation has been extended to the far infrared,[19–22] mid infrared,[23,24] and near infrared[3,4,6] spectral ranges. The HF dimer has also been subject to high level quantum chemical calculations, for example to obtain full dimensional potential energy hypersurfaces,[8,19,25–28] variational calculations,[29–33] and full dimensional Quantum Monte Carlo calculations.[19,20,34,35]

We also have developed a full dimensional potential energy hypersurface of high accuracy in the past (SO-3), where *ab initio* calculations have been refined by adjustment to spectroscopic data.[8] This allows detailed predictions about vibrationally excited states of $(HF)_2$ which are to be compared with experiment. Most recently two *ab initio* potentials have been recalculated at very high accuracy which seem to provide results comparable in quality to results from the SO-3 surface.[36,37,41]

The analysis of high-resolution infrared spectra of the vibrationally excited HF dimer provides information about the dynamics in highly-excited vibrational states, in particular concerning the predissociation of the hydrogen bond and the tunneling process of the hydrogen bond switching. It is then of special interest to investigate the influence of vibrational excitations on the hydrogen bond dynamics. It would be interesting, for example, to study mode-selective dynamics in the $N=2$ triad (first HF stretching overtone), where the HF-stretching vibration is excited by two quanta in three different ways, but with similar excitation energy: In the $N=2_3$ component, one quantum of HF-stretching excitation is essentially in the HF-donor and one quantum in the HF-acceptor unit, in $N=2_2$, both quanta are essentially in the HF-acceptor, and in $N=2_1$, both quanta are in the HF-donor unit. Unfortunately these overtone transitions are in general very weak and spectral congestion often prevents full assignment of overtone spectra in static cells.[3,6] Supersonic jet cooling can be very helpful to assign such spectra, but due to low number densities of $(HF)_2$ in a jet, transitions with very weak peak absorption could not be observed before. With conventional absorption techniques, only transitions to the $N_j=2_2$ component of the $N=2$ triad have been observed before in a supersonic jet and assigned.[42,43] We introduced cw-diode laser cavity ring-down spectroscopy in a pulsed supersonic slit jet expansion as a new high-resolution, high-sensitivity technique,[38,44–47] and we could observe and assign very weak transitions to the $N_j=2_1$ component.[38] In the present study, we report rovibrationally resolved spectra of the missing component $N_j=2_3$ and additional spectra of $N_j=2_2$. We can extract information about mode-selective hydrogen-bond predissociation and hydrogen-bond switching processes in these highly vibrationally excited states. Because now all three components of the $N=2$ triad have been observed and spectroscopically characterized, we can also resolve the long-standing question about the symmetry ordering of polyad levels in this overtone region and we can analyze the mode-selective dynamics in the $N=2$ triad in comparison with full-dimensional calculations on the SO-3 potential energy hypersurface and in comparison with previously published results of other polyads.

2. Experimental

We used our technique of cw-diode laser cavity ring-down spectroscopy in a pulsed supersonic slit jet expansion to

observe very weak overtone transitions of $(HF)_2$. A detailed description of this technique can be found in Refs. [38, 44–46], and only a short overview is given here: a tunable external cavity InGaAsP laser diode (Radians Innova) generated single-mode IR light near 1.3 μm (experimental bandwidth *ca.* 1 MHz, resolving power greater than 2×10^8). While part of the beam is used for a monitor étalon (500 MHz), the main part passes through an acousto-optical modulator (Isomet 1205C-2) after which the first-order deflection is coupled into an optical fiber, which guides the beam to the optical cavity set-up in a vacuum chamber. The stable optical cavity with length $l=32$ cm is composed of two highly reflective mirrors ($R \geq 99.97\%$). After switching-off the laser beam with the modulator, the decaying light intensity in the cavity is recorded by a fast photodetector (New Focus, 125 MHz) and fit to a single-exponential decay curve by a computer. Since light is reflected several thousand times inside the cavity, very long effective path lengths on the order of several km are obtained. From the ring-down constant k, the absorption coefficient α of the absorbing species present in the cavity can be derived from the relation $k=\alpha\ c+(1\text{-}R)\ c/l$, where c is the speed of light. The absorption per pass is defined as $A_{pp}=\alpha\ l$; it is a useful quantity when concentrations of the absorbing species are either non-uniform or unknown as in a supersonic jet expansion.

At a distance of 5 mm and carefully aligned along the optical axis of the cavity, a home-built pulsed solenoid slit valve[38,45,46,48,49] (33 mm × 0.1 mm) generates gas pulses of about 1.2 ms duration at a repetition rate between 5 and 10 Hz, while a diffusion pump backed by a roots-blower and roughing pump maintains a background pressure below 5×10^{-3} mbar in the vacuum chamber. The gas mixture consists of 4% HF (PanGas, ≥99.9%), 9% nitrous oxide N_2O (PanGas, ≥ 99.5%) to promote HF dimer formation,[38,42,50,51] and 87% argon (PanGas, ≥ 99.998%) as seeding gas at a backing pressure of 250 mbar. Mode-matching of the cavity length to the laser wavelength is achieved by a passive locking scheme, where one of the mirrors is mounted on a piezoelectric transducer to modulate periodically the cavity length by slightly more than one free spectral range. In the first modulation period, the nozzle is not operated. An optical resonance in this period is then used to predict when a resonance will occur in the second period. The nozzle is then opened accordingly so that the gas pulse will coincide with the predicted resonance. More details of this simple and robust mode-locking scheme are found in the Refs. [38, 44–46].

The recorded spectra are linearised using the fringes of the 500 MHz étalon and calibrated to absolute frequency by HF monomer transitions as spectroscopic reference lines[42,50] which were recorded simultaneously in a 10 cm absorption cell at room temperature. For the $N_j=2_2$, $K_a=0\leftarrow1$ transition we used the HF monomer line $P(3)$ at 7618.51907 cm^{-1}, for the $N_j=2_3$, $K_a=0\leftarrow0$ transition the HF $R(0)$ line at 7788.85535 cm^{-1}, and for the $N_j=2_3$, $K_a=1\leftarrow0$ transition the HF $R(1)$ line at 7823.81976 cm^{-1} for calibration. The calibrated spectra have an estimated absolute wavenumber uncertainty of less than 0.001 cm^{-1}.

3. Theory and Analysis of the Spectra

We performed variational calculations on HF dimer overtone transitions to the $N=2$ triad as described in Refs. [32,33] on the semiempirical overtone adjusted full-dimensional (6D) potential energy hypersurface (PES) SO-3.[8,28] Rovibrational energy levels are calculated by a sequential diagonalization/truncation scheme with a discrete variable representation of the intermolecular stretching coordinate.[52–54] The results of these calculations were used as predictions for the unknown band centers of the $N_j=2_3$ transitions and as guidance for the assignment of recorded spectra. Details of these calculations will be reported elsewhere.[32,33]

With an asymmetry parameter κ=-0.9998,[18,21,23] $(HF)_2$ is a nearly symmetric top. Energy levels in rovibrational spectra can be fit with good accuracy to Eq. (1),

$$\frac{E_{K_a}(J)}{hc} = \tilde{\nu}_{K_a} + \left(\bar{B}_{K_a} \pm \frac{1}{4}\delta_{K_a1} b_{K_a}\right) J(J+1) - \left[D_{K_a} \mp \left(\delta_{K_a1}+\delta_{K_a2}\right) d_{K_a}\right] J^2(J+1)^2 + \left[H_{K_a} \pm \left(\delta_{K_a2}+\delta_{K_a3}\right) h_{K_a}\right] J^3(J+1)^3, \quad (1)$$

where upper signs apply to $K_a+K_c=J$ and lower signs to $K_a+K_c=J+1$. $\tilde{\nu}_{K_a}$ is the hypothetical subband center for a given K_a level of a vibrational-tunneling state extrapolated to $J=0$, $\bar{B}_{K_a}=\left(B_{K_a}+C_{K_a}\right)/2$ denotes the average rotational constant, and asymmetry splitting terms are given by $b_{K_a}=\left(B_{K_a}-C_{K_a}\right)/2$, d_{K_a} and h_{K_a}, centrifugal distortion constants by D_{K_a} and H_{K_a}, and $\delta_{K_a i}(i=1,2,3)$ is the Kronecker delta.[20,22] Ground state spectroscopic parameters were taken from Refs. [20, 22, 55]. Relative line intensities in a subband are approximated by symmetric top Hönl-London formulae, where appropriate nuclear spin statistical weights have to be considered ($g_A=10$ for the symmetric (A) nuclear spin wavefunction combining with the symmetric (A) motional wavefunctions, and $g_B=6$ for the antisymmetric (B) nuclear spin wavefunction combining with the antisymmetric (B) motional wavefunctions).[20,21] Regarding pairwise permutation of nuclei, the total wavefunction has to satisfy the Pauli principle and the nuclear spin wavefunction Γ_n has accordingly either A^+ or B^+ symmetry. In our notation we follow Ref. [56] by assigning A to the state which is symmetric and B to the state which is antisymmetric with respect to monomer interchange. An upper index + or − for each state indicates positive or negative parity with respect to space inversion. In the tunneling process of the hydrogen bond switching in $(HF)_2$, the HF monomers interchange their role as hydrogen-bond donor and acceptor. Rovibrational transitions are thus split into two sublevels denoted by their tunneling-vibrational symmetry species Γ_{vt} in

the M_{S4} symmetry group. Each A' level in C_s symmetry (as the vibrational ground state or the vibrationally excited states involved in this study) is split by tunneling in a A^+/B^+ pair, and each A'' level in a A^-/B^- pair.[21,38,56] The total symmetry species Γ_{vtr} describes the symmetry of rovibrational levels of $(HF)_2$. It is the product of the tunneling-vibrational species Γ_{vt} and of the rotational species Γ_r. The optical electric dipole selection rules require a change of parity during a transition $(+ \leftrightarrow -)$ and conservation of nuclear spin symmetry $(A \nleftrightarrow B)$. Detailed discussions of the symmetry properties and character tables of the relevant groups can be found in Refs. [10, 21, 57].

As there is a great variety of nomenclatures for symmetry species in $(HF)_2$ quantum states, which can easily lead to confusion, we reproduce here for definiteness the character tables from Refs. [10, 21] which defines the notation used here (see Table 1). For a critical discussion of this aspect we refer to Refs. [10, 57].

The signed tunneling splitting is defined as the energy difference between the two tunneling sublevels,

$$\Delta\tilde{\nu}_T = \tilde{\nu}_{K_a}(\Gamma_{vt} = B^+) - \tilde{\nu}_{K_a}(\Gamma_{vt} = A^+). \quad (2)$$

The sign of the tunneling splitting, *i.e.* the symmetry ordering of the components in the $N=2$ triad, has been debated in several previous theoretical studies.[35,58–65] The long standing remaining open questions will be resolved in the present study by the experimental spectra in relation to high-level calculations. The tunneling splitting $\Delta\tilde{\nu}_T$ (in cm^{-1}) is related to the tunneling period τ_T by Equ. (3),

$$\tau_T = 1/(c\ |\Delta\tilde{\nu}_T|\ ) \quad (3)$$

The analysis of experimental rovibrational line shapes provides information about the predissociation dynamics of $(HF)_2$ in highly vibrationally excited levels. In the supersonic jet expansion, rovibrational lines are broadened essentially by two mechanisms, the Doppler-effect due to the effective translational temperature and beam divergence giving a Gaussian contribution, and predissociation of the dimer giving a Lorentzian contribution. The full width at half maximum (FWHM) of the Lorentzian line contribution $\Delta\tilde{\nu}_{PD}$ (in cm^{-1}) or $\Delta\nu_{PD}$ (in Hz) relates to the predissociation lifetime τ_{PD} as given by Equ. (4),[66]

$$\tau_{PD} = 1/(2\pi c\ \Delta\tilde{\nu}_{PD}) = 1/(2\pi\ \Delta\nu_{PD}). \quad (4)$$

The separation of the Gaussian and Lorentzian contribution to a line profile is achieved by a Voigt fit to the line. In a first step, an unconstrained non-linear least squares fit with a Voigt profile is applied to all lines of a given spectrum. From this an averaged value for the Gaussian contribution is obtained. In the final step, a constrained Voigt fit with the Gaussian contribution at the fixed averaged value yields the Lorentzian contribution to the line width for individual rovibrational lines. This fit procedure has been checked and validated by extensive numerical simulations (including also the effect of noise) in our previous publication, where more details can be found.[38] In those cases where the predissociation broadening is very large and dominates the total linewidths, we have used a simple Lorentzian fit, which may then overestimate the true Lorentzian contribution by 5–10%, well within the general uncertainty. Contributions from line broadening from spontaneous infrared emission and collisions are negligible in these experiments.

We note that in general the rotational distribution does not have to follow a strict Boltzmann distribution with a unique temperature in a supersonic jet expansion. Nevertheless, in the present experiments such a simple rotational distribution was indeed found to match the observation well, which is in fact quite frequently, but not always the case. Furthermore, the Doppler line shape does not necessarily have to fit a Gaussian, it can be quite different, even bimodal due to the contribution from geometric effects in the expansion. Again, in the present experiment, a Gaussian contribution fitted the lines of the co-expanding HF monomer, N_2O and the contribution to the Voigt profile in HF dimer very well, thus defining an apparent 'Doppler temperature'. This apparent translational temperature can be quite different from the rotational temperature, in particular it can be larger due to the geometric effects of the beam divergence, as is observed here. These effects are well

Table 1. Character tables for the symmetry groups of the HF dimer (HFHF).[10,21]

(a) Species	E	E^*	(ab) (13)(24)	$(ab)^*$ (13)(24)*	$\Gamma(M_{S4})\uparrow S^*_{2,2}$
A^+ (A_g)	1	1	1	1	$A_1^+ + A_2^+$
A^- (A_u)	1	−1	1	−1	$A_1^- + A_2^-$
B^+ (B_u)	1	1	−1	−1	$B_1^+ + B_2^+$
B^- (B_g)	1	−1	−1	1	$B_1^- + B_2^-$
(b) Species	E	(13)	(24)	(13)(24)	$(S_{2,2})\downarrow M_{S2}$
$A\times A\equiv A_1$	1	1	1	1	A
$B\times B\equiv A_2$	1	−1	−1	1	A
$B\times A\equiv B_1$	1	−1	1	−1	B
$A\times B\equiv B_{12}$	1	1	−1	−1	B

(a) Character table of the molecular symmetry group M_{S4} of $(HF)_2$; (b) Character table for $S_{2,2}$.

known and we refer to Refs. [67–72] for further discussion and some recent results.

4. Results and Discussion

Figure 1 in the introduction explains the polyad structure of the HF stretching overtone spectra. These spectra were measured even into the visible range up to the $N=4$ polyad,[6] although only limited analysis was possible at that time. The nomenclature N_j defines the total number of HF stretching quanta by N and gives the sublevels with index j in the order of increasing energy by convention. The polyad nomenclature is preferred as the excitation in none of the levels can be considered as strictly local. On the other hand, the approximate local mode nomenclature can help intuition, as it assigns a definite number of quanta to the 'bonded' and the 'free' HF stretching mode, for example $1+1$, $2+0$ or $0+2$ in the $N=2$ polyad. Figure 3 shows a survey of the 232 K FTIR spectrum of HF dimer[6,42] with the regions for the various polyad components in the $N_j=2_j$ polyad. While 2_1 and 2_2 could be roughly analysed already in 1989, and an accurate analysis of both components has been presented in Ref. [38], the analysis of the 2_3 component turned out to be the most difficult and is presented here.

4.1 The 2_1 Component

In the region of the $N=2$ triad (first HF stretching overtone), the $N=2_1$ component is the energetically lowest level. It corresponds to an excitation of the hydrogen bond donor mode with two HF stretching quanta. In our previous study, the first rovibrationally resolved and assigned spectrum corresponding to this component has been reported for the K_a $0\leftarrow0$ transition.[38] For convenience and to allow for a comparison with the other components of the $N=2$ triad, the main results are summarized here: The K_a $0\leftarrow0$ parallel transition has a band center at 7550.3555(26) cm^{-1} (values in parentheses are one standard deviation in the units of the last digit quoted), which corresponds to the origin of the $N=2_1$ component. Peak absorptions in this band are about $A_{pp}\approx10\times10^{-6}$, while the relative integrated band strength $\int A_{pp}\, d(\ln\tilde{\nu})$ is 4.9×10^{-9} cm. Since the absolute concentration in the supersonic jet is not known, only a relative integrated band strength can be quoted; it can be compared with other transitions, if equivalent experimental conditions apply. In the rovibrational spectrum, the tunneling splitting is clearly apparent in both the P- and R-branches. The splitting $\Delta\tilde{\nu}_T=0.0150(37)$ cm^{-1} corresponds to a tunneling period of 2.22(55) ns. From an analysis of rovibrational line shapes, a predissociation line width $\Delta\nu_{PD}$ of 3.11(34) GHz is determined for the lower tunneling state $\Gamma_{vt}=A^+$ and 3.25(69) GHz for the upper tunneling state $\Gamma_{vt}=B^+$, equivalent to predissociation lifetimes τ_{PD} of 51.2(56) ps for A^+ and 49(10) ps for B^+.

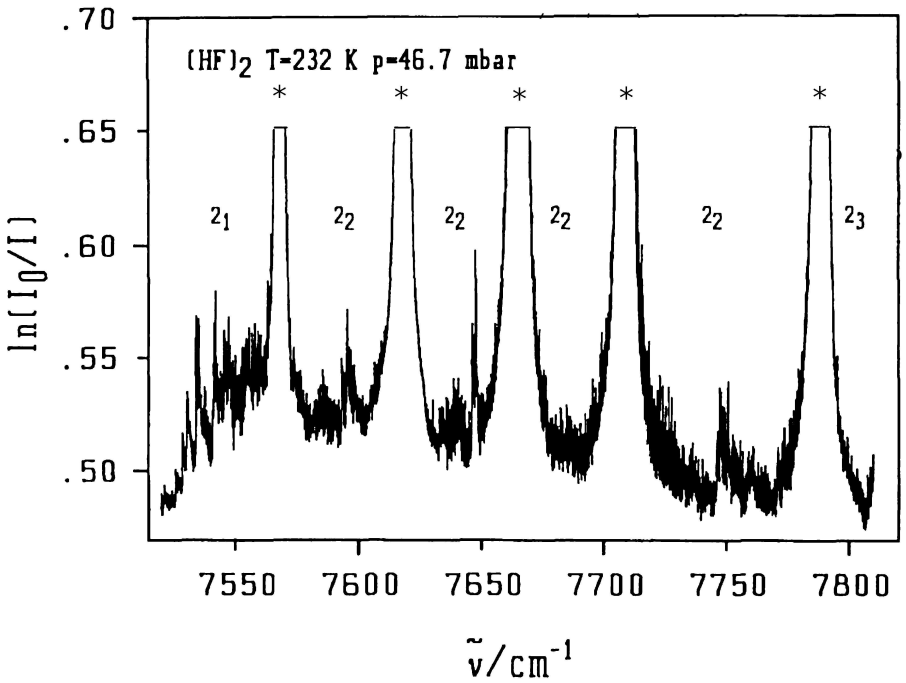

Figure 3. Survey of the 232 K FTIR spectrum of the HF dimer with the regions of the N_j polyad components indicated (after Refs. [6,42]). The peaks marked with an asterisk are HF monomer lines (truncated at the absorbance value ln $(I_0/I)=0.65$).

4.2 The 2_2 Component

In the energetically intermediate component $N=2_2$, the hydrogen bond acceptor mode is excited by two HF stretching quanta. In our previous publication, we presented the rovibrationally resolved and assigned spectrum of the K_a 1←0 perpendicular transition to this component;[38] in the meantime, we also observed the K_a 0←1 perpendicular hot-band transition (see Figure 4), which allows the determination of the origin of the $N=2_2$ component and also allows the study of the influence of K_a excitation on the dynamics in this component. For the K_a 1←0 perpendicular transition, the rovibrational analysis provided the band center at 7711.37956(66) cm^{-1} and a tunneling splitting $\Delta\tilde{\nu}_T =$ 0.0936(10) cm^{-1} corresponding to a tunneling period of 0.3561(38) ns.[38] A line shape analysis yielded a Lorentzian line width of 121(12) MHz for the $\Gamma_{vt}=A^+$ sublevel and 84(11) MHz for $\Gamma_{vt}=B^+$ which is attributed to predissociation. The corresponding predissociation lifetimes are then 1.32(13) ns and 1.89(25) ns for the $\Gamma_{vt}=A^+$ and B^+ sublevels, respectively.[38] With peak absorptions of $A_{pp}\approx 100\times10^{-6}$, this transition has the strongest peak intensities within the $N=2$ triad. The relative integrated band strength is determined as 3.9×10^{-9} cm, which is comparable to the K_a 0←0 parallel transition of the $N=2_1$ component (see above); the much higher peak intensities here are thus mainly due to much narrower line widths.

In the present study, we could also analyze the K_a 0←1 perpendicular hot-band transition to $N=2_2$. In Figure 4, the corresponding jet-cooled spectrum is shown. The observed peak absorptions are about $A_{pp}\approx 33\times10^{-6}$, and the integrated relative band strength is 8.3×10^{-10} cm. A rotational temperature of *ca.* 27.0(8) K applies to the HF dimer in the jet under the present experimental conditions. In the figure, the experimental spectrum (bottom trace) is compared with a simulation (middle trace), and the rotational assignment is presented (top trace). The agreement between experimental spectrum and simulation is excellent. The clearly visible intensity alternation from the nuclear spin statistics provides further support for the assignment. Peak positions from the

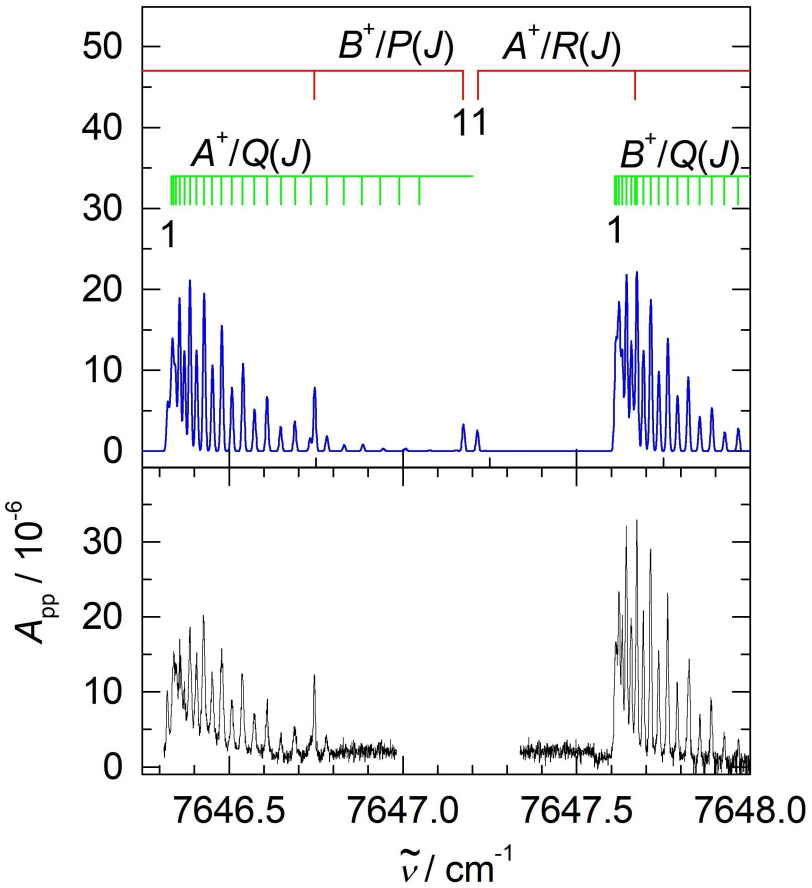

Figure 4. *Q*-branch region of the $N_j=2_2$, $K_a=0\leftarrow1$ transition of $(HF)_2$. Lower part: experimental CRD spectrum in the slit jet expansion. Upper part: simulation for a rotational temperature of 27 K and assignment where the labels A^+ or B^+ denote rotational branches terminating in the $\Gamma_{vt}=A^+$ or B^+ tunneling sublevel of the vibrationally excited state, respectively. The simulation is carried out with a Voigt line shape corresponding to a Lorentzian width of 100 MHz (FWHM) and a Gaussian contribution with 167 MHz (FWHM; formal translational temperature 45 K).

experimental spectrum and the rotational assignment of 35 lines are given in Table 2, in addition to a comparison with calculated line positions. The term value of the upper level of this transition is determined to be 7682.8178(12) cm^{-1}, which corresponds to the origin of the $N=2_2$ component. The rovibrational analysis provided a tunneling splitting of $\Delta\tilde{\nu}_T =$ 0.2156(18) cm^{-1} corresponding to a tunneling period of 0.1546(13) ns; in $K_a=0$ of $N=2_2$, tunneling dynamics is thus about two times faster than in $K_a=1$. The remaining spectroscopic parameters obtained by the rovibrational analysis are summarized in Table 3.

The 2_2 ($K=0$) level has been studied and analyzed several times in the past with different data sets providing slightly differing results.[3,6,38,42,43] For example, the tunneling splitting $\Delta\tilde{\nu}_T$ was found to be 0.2 cm^{-1} in an approximate early analysis of FTIR spectra,[3,6] 0.2120 cm^{-1} in direct absorption supersonic jet spectra[43] and also in further supersonic jet spectra 0.2116 cm^{-1},[42] which differ slightly outside the statistical spread from the current values. However, these slight differences can arise from systematic effects due to different sets of rotational levels observed and the results should be considered consistent.

Variational calculations on the SO-3 potential energy hypersurface give a term value of the lower tunneling sublevel

Table 3. Spectroscopic parameters of the $K_a=0$ level of the $N_j=2_2$ band of $(HF)_2$.[a)]

Parameter	$\Gamma_{vt}=A^+$	$\Gamma_{vt}=B^+$
$\tilde{\nu}/cm^{-1}$	7682.8178(12)	7683.0334(12)
$\Delta\tilde{\nu}_T/cm^{-1}$	0.2156(18)	
B/cm^{-1}	0.219895(39)	0.219810 (38)
$D/10^{-6}$ cm^{-1}	2.60(29)	1.93(25)
$H/10^{-12}$ cm^{-1}	800(58)	−250(45)
$N_{data}=35$	$D_{RMS}=1.9\times10^{-3}$ cm^{-1}	

[a)] Values in parentheses represent one standard deviation in the units of the last digit quoted. Refs. [42, 43] give slightly different results which are, however, consistent with the present results given systematic differences from different data sets (see main text for discussion).

Table 2. Observed and calculated line positions for the $N_j=2_2$, $K_a=0\leftarrow1$ transition.

Γ_{vtr}	Γ_r	Γ_{vt}	J_{K_a,K_c}	←	Γ_{vtr}	Γ_r	Γ_{vt}	J_{K_a,K_c}	g_k	$\tilde{\nu}_{obs}/cm^{-1}$	Δ_{o-c}
B^-	B^-	A^+	$1_{0,1}$	←	B^+	A^+	B^+	$1_{1,0}$	6	7646.3228	−83
A^+	A^+	A^+	$2_{0,2}$	←	A^-	B^-	B^+	$2_{1,1}$	10	7646.3401	32
B^-	B^-	A^+	$3_{0,3}$	←	B^+	A^+	B^+	$3_{1,2}$	6	7646.3503	49
A^+	A^+	A^+	$4_{0,4}$	←	A^-	B^-	B^+	$4_{1,3}$	10	7646.3569	2
B^-	B^-	A^+	$5_{0,5}$	←	B^+	A^+	B^+	$5_{1,4}$	6	7646.3716	10
A^+	A^+	A^+	$6_{0,6}$	←	A^-	B^-	B^+	$6_{1,5}$	10	7646.3880	7
B^-	B^-	A^+	$7_{0,7}$	←	B^+	A^+	B^+	$7_{1,6}$	6	7646.4064	0
A^+	A^+	A^+	$8_{0,8}$	←	A^-	B^-	B^+	$8_{1,7}$	10	7646.4271	−10
B^-	B^-	A^+	$9_{0,9}$	←	B^+	A^+	B^+	$9_{1,8}$	6	7646.4515	−9
A^+	A^+	A^+	$10_{0,10}$	←	A^-	B^-	B^+	$10_{1,9}$	10	7646.4793	2
B^-	B^-	A^+	$11_{0,11}$	←	B^+	A^+	B^+	$11_{1,10}$	6	7646.5081	0
A^+	A^+	A^+	$12_{0,12}$	←	A^-	B^-	B^+	$12_{1,11}$	10	7646.5387	−7
B^-	B^-	A^+	$13_{0,13}$	←	B^+	A^+	B^+	$13_{1,12}$	6	7646.5728	−4
A^+	A^+	A^+	$14_{0,14}$	←	A^-	B^-	B^+	$14_{1,13}$	10	7646.6092	−2
B^-	B^-	A^+	$15_{0,15}$	←	B^+	A^+	B^+	$15_{1,14}$	6	7646.6493	12
A^+	A^+	A^+	$16_{0,16}$	←	A^-	B^-	B^+	$16_{1,15}$	10	7646.6892	−1
B^-	B^-	A^+	$17_{0,17}$	←	B^+	A^+	B^+	$17_{1,16}$	6	7646.7342	7
A^+	A^+	A^+	$18_{0,18}$	←	A^-	B^-	B^+	$18_{1,17}$	10	7646.7799	−6
A^-	B^-	B^+	$1_{0,1}$	←	A^+	A^+	A^+	$2_{1,2}$	10	7646.7455	0
A^-	B^-	B^+	$3_{0,3}$	←	A^+	A^+	A^+	$3_{1,2}$	10	7647.6227	4
B^+	A^+	B^+	$4_{0,4}$	←	B^-	A^+	A^+	$4_{1,3}$	6	7647.6314	0
A^-	B^-	B^+	$5_{0,5}$	←	A^+	A^+	A^+	$5_{1,4}$	10	7647.6429	−1
B^+	A^+	B^+	$6_{0,6}$	←	B^-	B^-	A^+	$6_{1,5}$	6	7647.6571	0
A^-	B^-	B^+	$7_{0,7}$	←	A^+	A^+	A^+	$7_{1,6}$	10	7647.6731	−1
B^+	A^+	B^+	$8_{0,8}$	←	B^-	B^-	A^+	$8_{1,7}$	6	7647.6918	−1
A^-	B^-	B^+	$9_{0,9}$	←	A^+	A^+	A^+	$9_{1,8}$	10	7647.7129	0
B^+	A^+	B^+	$10_{0,10}$	←	B^-	B^-	A^+	$10_{1,9}$	6	7647.7359	−4
A^-	B^-	B^+	$11_{0,11}$	←	A^+	A^+	A^+	$11_{1,10}$	10	7647.7618	−3
B^+	A^+	B^+	$12_{0,12}$	←	B^-	B^-	A^+	$12_{1,11}$	6	7647.7895	−7
A^-	B^-	B^+	$13_{0,13}$	←	A^+	A^+	A^+	$13_{1,12}$	10	7647.8227	20
B^+	A^+	B^+	$14_{0,14}$	←	B^-	B^-	A^+	$14_{1,13}$	6	7647.8548	12
A^-	B^-	B^+	$15_{0,15}$	←	A^+	A^+	A^+	$15_{1,14}$	10	7647.8876	−10
B^+	A^+	B^+	$16_{0,16}$	←	B^-	B^-	A^+	$16_{1,15}$	6	7647.9249	−9
B^+	A^+	B^+	$18_{0,18}$	←	B^-	B^-	A^+	$18_{1,17}$	6	7648.0071	1
A^-	B^-	B^+	$19_{0,19}$	←	A^+	A^+	A^+	$19_{1,18}$	10	7648.0506	1

Γ_{vt} gives the tunneling-vibrational symmetry and J, K_a and K_c are the rotational quantum numbers. g_k is the spin statistical weight. $\Delta_{o-c}=(\tilde{\nu}_{obs}-\tilde{\nu}_{calc})/10^{-4}$ cm^{-1} is the difference between observed and calculated positions.

7679.767 cm^{-1} for $N=2_2$ and a tunneling splitting of 0.207 cm^{-1}. These calculated values are in reasonable agreement with the experimental values. From a line shape analysis, the predissociation line width is obtained as the Lorentzian contribution to the Voigt profile (Gaussian contribution fixed at 167 MHz, FWHM), yielding an averaged predissociation line width (FWHM) of 146(21) MHz from 7 lines of the $\Gamma_{vt}=A^+$ tunneling sublevel and 88(14) MHz from 5 lines of $\Gamma_{vt}=B^+$. The numbers in parentheses provide the spread of line widths as one standard deviation in the units of the last digit quoted; they thus include both the experimental uncertainty and the possible spread of widths of individual lines. These values are in agreement with previously published values of 175(25) MHz for $\Gamma_{vt}=A^+$ and 56(20) MHz for $\Gamma_{vt}=B^+$.[43] The present results correspond to a predissociation lifetime τ_{PD} of 1.09(15) ns for $\Gamma_{vt}=A^+$ and 1.80(29) ns for $\Gamma_{vt}=B^+$. Predissociation lifetimes in $K_a=0$ and in $K_a=1$ of $N_j=2_2$ are thus very similar.

4.3 The 2_3 Component

The last member of the $N=2$ triad is the $N=2_3$ component; it is described by one quantum of HF-stretching excitation in the HF-donor and one quantum in the HF-acceptor unit. A comparable situation, where both units of the dimer are excited simultaneously with the same amount of quanta, does not exist for the other polyads studied in detail so far, $N=1$ (Refs. [23,24]) and $N=3$ (Refs. [73–75]). The analysis of transitions to $N=2_3$ thus provides the opportunity to study an interesting effect from the influence of this equal simultaneous vibrational excitation on the dynamics. In this investigation, we were able to observe, analyze, and assign the parallel K_a 0←0 transition and the perpendicular K_a 1←0 transition to the $N=2_3$ component of jet-cooled $(HF)_2$.

The experimental spectrum of the parallel K_a 0←0 transition is shown in Figure 5, where also a simulation and the rotational assignments are given. The spectrum is characterized by rather small peak absorbances of $A_{pp}\approx 7\times 10^{-6}$, while the relative integrated band strength determined from the simulation is about 6.9×10^{-10} cm. In the experimental spectrum, there are also additional, very narrow lines, for

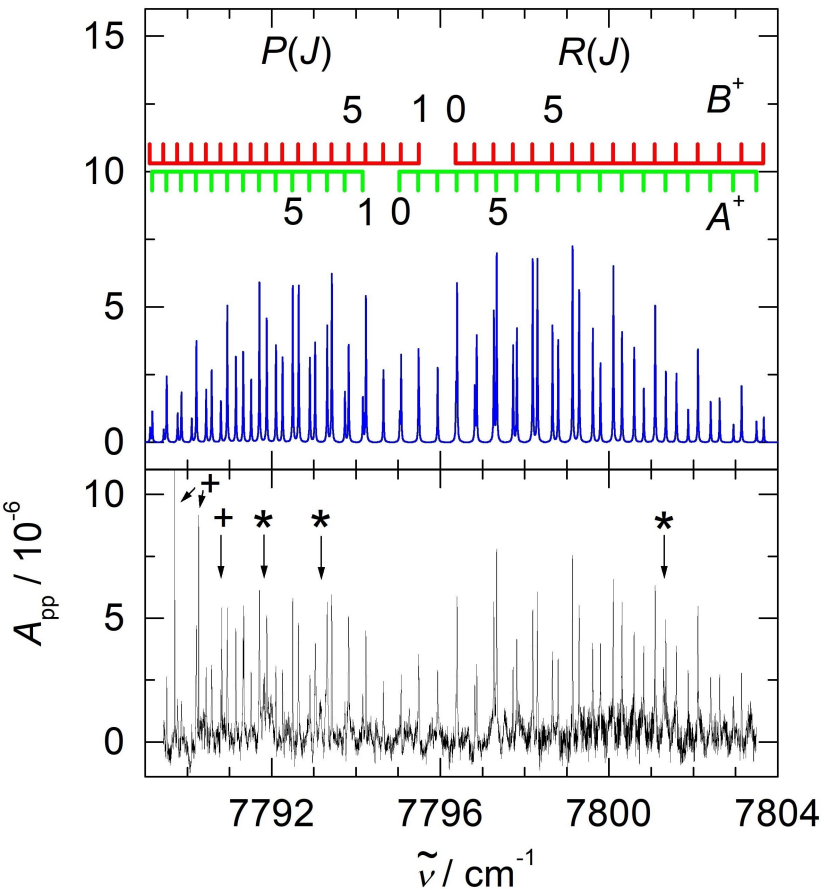

Figure 5. $N_j=2_3$, $K_a=0$←0 transition of $(HF)_2$. Lower part: experimental CRD spectrum in the slit jet expansion. Additional broad transitions, which are not due to that vibrational band, are marked with an asterisk, narrow transitions due to N_2O with a plus sign. Upper part: simulation for a rotational temperature of 26 K (using a Lorentzian line profile for the $(HF)_2$ lines) and assignment.

example the two intense features at the low-wavenumber side in Figure 5; they are due to nitrous oxide, which is also present in the supersonic expansion. The $(HF)_2$ spectrum is dominated by *P*- and *R*-branch transitions, which are divided into the two tunneling-split subbands. The intensity alternation due to the different nuclear spin statistical weights is clearly apparent. The rotational analysis provided the rotational assignment and spectroscopic constants. Peak positions from the experimental spectrum and the rotational assignment of 55 lines are given in Table 4, in addition to a comparison with calculated line positions.

In Table 5 the spectroscopic constants of the parallel K_a 0←0 transition are summarized. Using these parameters, the spectrum has been simulated assuming a rotational temperature of 26 K; the agreement between experiment and simulation is very satisfactory, in particular considering the unfavorable experimental signal-to-noise ratio due to low peak intensities. The band center has been determined as 7795.2546(7) cm^{-1}, which corresponds to the origin of the $N=2_3$ component. The tunneling splitting in $K_a=0$ of $N=2_3$ is $\Delta\tilde{\nu}_T=0.6761(11)$ cm^{-1}, which relates to a very short tunneling time of $\tau_T=49.30(8)$ ps. Variational calculations on the SO-3 potential energy hypersurface provided a band center at 7795.255 cm^{-1} and a tunneling splitting of 0.473 cm^{-1}, which are both in reasonable agreement with the experimental values. In Table 4 the line widths of 47 individual lines of this band are listed. The resulting predissociation line widths (FWHM) in the individual tunneling sublevels are 500(100) MHz for $\Gamma_{vt}=A^+$ and 470(70) MHz for $\Gamma_{vt}=B^+$. This corresponds to predissociation lifetimes of $\tau_{PD}=320(70)$ ps for $\Gamma_{vt}=A^+$ and $\tau_{PD}=340(50)$ ps for $\Gamma_{vt}=B^+$ in the $K_a=0$ level of the $N_j=2_3$ component. The numbers given in parentheses provide the spread of lifetimes in terms of one standard deviation in units of the last digit quoted. They thus include both the experimental statistical uncertainty and the systematic spread for different rotational states.

In Figure 6 the experimental spectrum of the perpendicular K_a 1←0 transition is shown and compared with a simulation, where the spectroscopic parameters from a rotational analysis (summarized in Table 6 and Table 7) have been used and a rotational temperature of 27 K has been assumed. The agreement between experiment and simulation is good. In Table 6 peak positions and rotational assignments of 37 lines are listed, including a comparison with calculated line positions. With $A_{pp}\approx 3\times10^{-6}$, this transition has the weakest peak absorbances of all transitions to the $N=2$ triad studied in this work. The

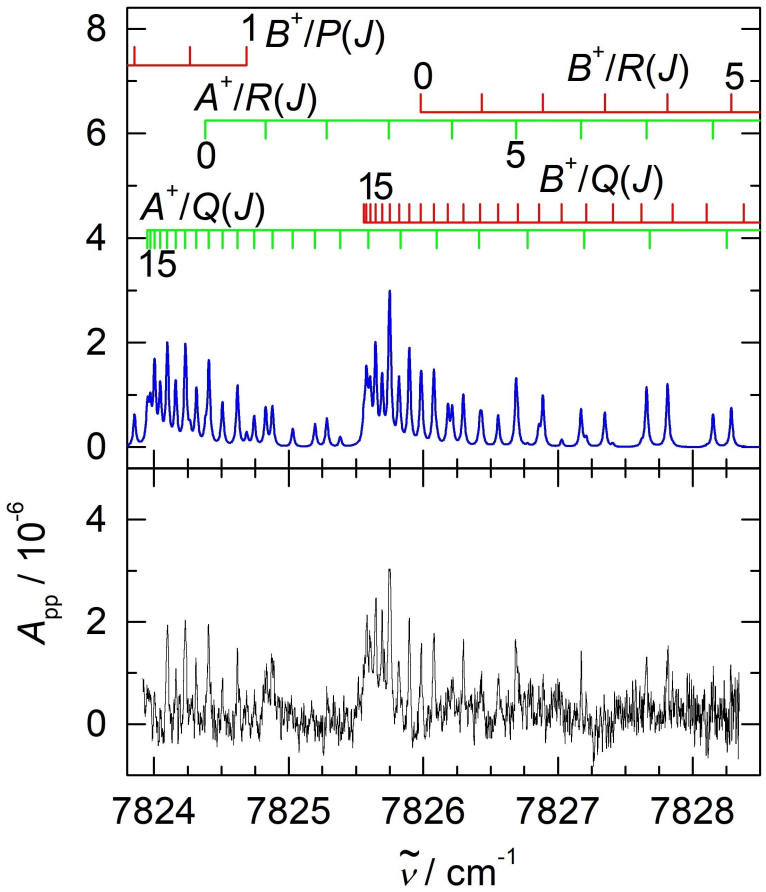

Figure 6. $N_j=2_3$, $K_a=1\leftarrow0$ transition of $(HF)_2$. Lower part: experimental CRD spectrum in the slit jet expansion. Upper part: simulation for a rotational temperature of 26 K and assignment.

Table 4. Observed and calculated line positions for the $N_j = 2_3$, $K_a = 0 \leftarrow 0$ transition, with assignment and with experimentally determined predissociation line widths $\Delta\tilde{\nu}_{PD}$ (FWHM) from a fit to a Lorentzian profile (neglecting the Gaussian contribution). J, K_a and K_c are the rotational quantum numbers. Γ_r is the rotational species, Γ_{vt} the tunneling-vibrational species and $\Gamma_{vtr} = \Gamma_{vt} \times \Gamma_r$ the total symmetry species. g_k is the spin statistical weight. $\Delta_{o-c} = (\tilde{\nu}_{obs} - \tilde{\nu}_{calc})/10^{-4}$ cm^{-1} is the difference between the observed and calculated position. Values in parentheses represent one standard deviation in the units of the last digit quoted.

a) P—Branch Transitions

Γ_{vtr}	Γ_r	Γ_{vt}	J_{K_a,K_c}	←	Γ_{vtr}	Γ_r	Γ_{vt}	J_{K_a,K_c}	g_k	$\tilde{\nu}_{obs}$/cm^{-1}	Δ_{o-c}	$\Delta\tilde{\nu}_{PD}$/cm^{-1}
A^+	A^+	A^+	$12_{0,12}$	←	A^-	B^-	B^+	$13_{0,13}$	10	7789.5097	−1	0.01471(79)
B^-	B^-	A^+	$11_{0,11}$	←	B^+	A^+	B^+	$12_{0,12}$	6	7789.8598	17	0.0164(18)
A^+	A^+	A^+	$10_{0,10}$	←	A^-	B^-	B^+	$11_{0,11}$	10	7790.2135	−2	0.01940(86)
A^-	B^-	B^+	$13_{0,13}$	←	A^+	A^+	A^+	$14_{0,14}$	10	7790.4454	−3	0.0134(14)
B^-	B^-	A^+	$9_{0,9}$	←	B^+	A^+	B^+	$10_{0,10}$	6	7790.5759	−7	0.0206(12)
B^+	A^+	B^+	$12_{0,12}$	←	B^-	B^-	A^+	$13_{0,13}$	6	7790.7941	−3	0.0115(11)
A^+	A^+	A^+	$8_{0,8}$	←	A^-	B^-	B^+	$9_{0,9}$	10	7790.9472	5	0.01871(63)
A^-	B^-	B^+	$11_{0,11}$	←	A^+	A^+	A^+	$12_{0,12}$	10	7791.1492	−8	0.01523(46)
B^-	B^-	A^+	$7_{0,7}$	←	B^+	A^+	B^+	$8_{0,8}$	6	7791.3223	−16	0.01473(84)
B^+	A^+	B^+	$10_{0,10}$	←	B^-	B^-	A^+	$11_{0,11}$	6	7791.5125	1	0.01275(75)
A^+	A^+	A^+	$6_{0,6}$	←	A^-	B^-	B^+	$7_{0,7}$	10	7791.7097	12	0.01932(74)
A^-	B^-	B^+	$9_{0,9}$	←	A^+	A^+	A^+	$10_{0,10}$	10	7791.8867	52	0.0167(11)
B^-	B^-	A^+	$5_{0,5}$	←	B^+	A^+	B^+	$6_{0,6}$	6	7792.1011	10	0.01227(76)
B^+	A^+	B^+	$8_{0,8}$	←	B^-	B^-	A^+	$9_{0,9}$	6	7792.2560	−12	0.01354(95)
A^+	A^+	A^+	$4_{0,4}$	←	A^-	B^-	B^+	$5_{0,5}$	10	7792.4983	−4	0.01368(52)
A^-	B^-	B^+	$7_{0,7}$	←	A^+	A^+	A^+	$8_{0,8}$	10	7792.6385	−11	0.01481(51)
B^-	B^-	A^+	$3_{0,3}$	←	B^+	A^+	B^+	$4_{0,4}$	6	7792.9057	14	0.01534(15)
B^+	A^+	B^+	$6_{0,6}$	←	B^-	B^-	A^+	$7_{0,7}$	6	7793.0330	45	–
A^+	A^+	A^+	$2_{0,2}$	←	A^-	B^-	B^+	$3_{0,3}$	10	7793.3160	−8	–
A^-	B^-	B^+	$5_{0,5}$	←	A^+	A^+	A^+	$6_{0,6}$	10	7793.4242	2	0.01428(55)
B^-	B^-	A^+	$1_{0,1}$	←	B^+	A^+	B^+	$2_{0,2}$	6	7793.7349	−15	0.0121(25)
B^+	A^+	B^+	$4_{0,4}$	←	B^-	B^-	A^+	$5_{0,5}$	6	7793.8250	−10	–
A^+	A^+	A^+	$0_{0,0}$	←	A^-	B^-	B^+	$1_{0,1}$	10	7794.1620	−7	–
A^-	B^-	B^+	$3_{0,3}$	←	A^+	A^+	A^+	$4_{0,4}$	10	7794.2347	4	0.01332(54)
B^+	A^+	B^+	$2_{0,2}$	←	B^-	B^-	A^+	$3_{0,3}$	6	7794.6500	10	–
A^-	B^-	B^+	$1_{0,1}$	←	A^+	A^+	A^+	$2_{0,2}$	10	7795.0687	−13	–

b) R—Branch Transitions

Γ_{vtr}	Γ_r	Γ_{vt}	J_{K_a,K_c}	←	Γ_{vtr}	Γ_r	Γ_{vt}	J_{K_a,K_c}	g_k	$\tilde{\nu}_{obs}$/cm^{-1}	Δ_{o-c}	$\Delta\tilde{\nu}_{PD}$/cm^{-1}
A^+	A^+	A^+	$2_{0,2}$	←	A^-	B^-	B^+	$1_{0,1}$	10	7795.4830	6	–
B^-	B^-	A^+	$3_{0,3}$	←	B^+	A^+	B^+	$2_{0,2}$	6	7795.9372	16	0.0201(13)
A^+	A^+	A^+	$4_{0,4}$	←	A^-	B^-	B^+	$3_{0,3}$	10	7796.3955	0	0.0207(11)
B^+	A^+	B^+	$2_{0,2}$	←	B^-	B^-	A^+	$1_{0,1}$	6	7796.8166	8	0.0203(13)
B^-	B^-	A^+	$5_{0,5}$	←	B^+	A^+	B^+	$4_{0,4}$	6	7796.8624	5	0.01781(83)
A^-	B^-	B^+	$3_{0,3}$	←	A^+	A^+	A^+	$2_{0,2}$	10	7797.2682	7	0.01838(24)
A^+	A^+	A^+	$6_{0,6}$	←	A^-	B^-	B^+	$5_{0,5}$	10	7797.3347	−2	0.01437(43)
B^+	A^+	B^+	$4_{0,4}$	←	B^-	B^-	A^+	$3_{0,3}$	6	7797.7217	−35	0.0152(13)
B^-	B^-	A^+	$7_{0,7}$	←	B^+	A^+	B^+	$6_{0,6}$	6	7797.8125	−18	0.0139(12)
A^-	B^-	B^+	$5_{0,5}$	←	A^+	A^+	A^+	$4_{0,4}$	10	7798.1901	12	0.01837(93)
A^+	A^+	A^+	$8_{0,8}$	←	A^-	B^-	B^+	$7_{0,7}$	10	7798.3010	9	0.01471(78)
B^+	A^+	B^+	$6_{0,6}$	←	B^-	B^-	A^+	$5_{0,5}$	6	7798.6576	−9	0.01524(79)
B^-	B^-	A^+	$9_{0,9}$	←	B^+	A^+	B^+	$8_{0,8}$	6	7798.7908	−15	0.01215(63)
A^-	B^-	B^+	$7_{0,7}$	←	A^+	A^+	A^+	$6_{0,6}$	10	7799.1349	10	0.01397(53)
A^+	A^+	A^+	$10_{0,10}$	←	A^-	B^-	B^+	$9_{0,9}$	10	7799.2914	6	0.01869(97)
B^+	A^+	B^+	$8_{0,8}$	←	B^-	B^-	A^+	$7_{0,7}$	6	7799.6134	−18	0.0160(13)
B^-	B^-	A^+	$11_{0,11}$	←	B^+	A^+	B^+	$10_{0,10}$	6	7799.7954	−1	0.0142(13)
A^-	B^-	B^+	$9_{0,9}$	←	A^+	A^+	A^+	$8_{0,8}$	10	7800.0998	−24	0.01572(88)
A^+	A^+	A^+	$12_{0,12}$	←	A^-	B^-	B^+	$11_{0,11}$	10	7800.3064	1	0.0170(12)
B^+	A^+	B^+	$10_{0,10}$	←	B^-	B^-	A^+	$9_{0,9}$	6	7800.5936	−14	0.0162(14)
B^-	B^-	A^+	$13_{0,13}$	←	B^+	A^+	B^+	$12_{0,12}$	6	7800.8233	0	0.01153(13)
A^-	B^-	B^+	$11_{0,11}$	←	A^+	A^+	A^+	$10_{0,10}$	10	7801.0939	4	0.0192(12)
A^+	A^+	A^+	$14_{0,14}$	←	A^-	B^-	B^+	$13_{0,13}$	10	7801.3455	−8	0.0207(17)
B^+	A^+	B^+	$12_{0,12}$	←	B^-	B^-	A^+	$11_{0,11}$	6	7801.5962	−14	0.0167(15)
B^-	B^-	A^+	$15_{0,15}$	←	B^+	A^+	B^+	$14_{0,14}$	6	7801.8756	4	–
A^-	B^-	B^+	$13_{0,13}$	←	A^+	A^+	A^+	$12_{0,12}$	10	7802.1086	14	0.01613(87)
A^+	A^+	A^+	$16_{0,16}$	←	A^-	B^-	B^+	$15_{0,15}$	10	7802.4100	0	0.0238(12)
B^+	A^+	B^+	$14_{0,14}$	←	B^-	B^-	A^+	$13_{0,13}$	6	7802.6239	16	0.0159(14)
A^-	B^-	B^+	$15_{0,15}$	←	A^+	A^+	A^+	$14_{0,14}$	10	7803.1417	−10	0.01853(69)

Table 5. Spectroscopic parameters of the $K_a=0$ level of the $N_j=2_3$ band of $(HF)_2$.[a)]

Parameter	$\Gamma_{vt}=A^+$	$\Gamma_{vt}=B^+$
$\tilde{\nu}$/cm^{-1}	7795.25457 (70)	7795.93067 (70)
$\Delta\tilde{\nu}_T$/cm^{-1}	0.6761 (11)	
B/cm^{-1}	0.219953 (29)	0.219782 (36)
$D/10^{-6}$ cm^{-1}	2.02 (29)	1.96 (38)
$H/10^{-12}$ cm^{-1}	−160 (74)	−300 (110)
$N_{data}=55$	$D_{RMS}=1.5\times10^{-3}$ cm^{-1}	

[a)] Values in parentheses represent one standard deviation in the units of the last digit quoted.

relative integrated band strength of the perpendicular K_a 1←0 transition is 2.3×10^{-10} cm. In the spectrum, Q-branch transitions are dominant, but some R-branch and very few P-branch transitions are also apparent. The intensity alternation due to the different nuclear spin statistical weights and the tunneling splitting into two subbands is clearly visible in the spectrum, in particular in the dominating Q-branch. The band center has been determined at 7824.5977(16) cm^{-1}. The tunneling splitting of 0.9492(22) cm^{-1} in this band corresponds to a very short tunneling time of 35.12(8) ps. From a line shape analysis of 16 selected rovibrational lines (Lorentzian fits), predissociation line widths (FWHM) have been determined for both tunneling states (see Table 6), 630(100) MHz for the $\Gamma_{vt}=B^+$ tunneling sublevel and 660(130) MHz for $\Gamma_{vt}=A^+$. This relates to predissociation lifetimes of $\tau_{PD}=$ 240(50) ps for $\Gamma_{vt}=A^+$ and $\tau_{PD}=250(40)$ ps for $\Gamma_{vt}=B^+$ in the vibrationally excited $K_a=1$ state of $N_j=2_3$.

Table 6. Observed and calculated line positions for the $N_j=2_3$, $K_a=1\leftarrow0$ transition. Γ_{vt} gives the tunneling-vibrational symmetry and J, K_a and K_c are the rotational quantum numbers. g_k is the spin statistical weight. $\Delta_{o-c}=(\tilde{\nu}_{obs}-\tilde{\nu}_{calc})/10^{-4}$ cm^{-1} is the difference between observed and calculated positions. Experimentally determined predissociation line widths $\Delta\tilde{\nu}_{PD}$ (FWHM) from a fit to a Lorentzian profile (neglecting the Gaussian contribution).

Γ_{vtr}	Γ_r	Γ_{vt}	J_{K_a,K_c}	←	Γ_{vtr}	Γ_r	Γ_{vt}	J_{K_a,K_c}	g_k	$\tilde{\nu}_{obs}$/cm−1	Δ_{o-c}	$\Delta\tilde{\nu}_{PD}$/cm^{-1}
A^+	A^+	A^+	$1_{1,0}$	←	A^-	B^-	B^+	$1_{0,1}$	10	7823.9499	1	0.0229(16)
B^-	B^-	A^+	$2_{1,1}$	←	B^+	A^+	B^+	$2_{0,2}$	6	7823.9670	−41	–
A^+	A^+	A^+	$3_{1,2}$	←	A^-	B^-	B^+	$3_{0,3}$	10	7824.0031	1	–
B^-	B^-	A^+	$4_{1,3}$	←	B^+	A^+	B^+	$4_{0,4}$	6	7824.0470	17	–
A^+	A^+	A^+	$5_{1,4}$	←	A^-	B^-	B^+	$5_{0,5}$	10	7824.0998	21	–
B^-	B^-	A^+	$6_{1,5}$	←	B^+	A^+	B^+	$6_{0,6}$	6	7824.1625	24	–
A^+	A^+	A^+	$7_{1,6}$	←	A^-	B^-	B^+	$7_{0,7}$	10	7824.2314	−8	0.0256(20)
B^-	B^-	A^+	$8_{1,7}$	←	B^+	A^+	B^+	$8_{0,8}$	6	7824.3100	−40	–
A^+	A^+	A^+	$9_{1,8}$	←	A^-	B^-	B^+	$9_{0,9}$	10	7824.4034	−22	0.0203(19)
B^-	B^-	A^+	$10_{1,9}$	←	B^+	A^+	B^+	$10_{0,10}$	6	7824.5089	17	0.0153(25)
A^+	A^+	A^+	$11_{1,10}$	←	A^-	B^-	B^+	$11_{0,11}$	10	7824.6202	10	0.0273(44)
A^-	B^-	B^+	$1_{1,1}$	←	A^+	A^+	A^+	$2_{0,2}$	10	7824.6851	−18	–
B^-	B^-	A^+	$12_{1,11}$	←	B^+	A^+	B^+	$12_{0,12}$	6	7824.7444	18	–
A^+	A^+	A^+	$2_{1,2}$	←	A^-	B^-	B^+	$1_{0,1}$	10	7824.8274	−1	–
A^+	A^+	A^+	$13_{1,12}$	←	A^-	B^-	B^+	$13_{0,13}$	10	7824.8771	−14	–
B^-	B^-	A^+	$3_{1,3}$	←	B^+	A^+	B^+	$2_{0,2}$	6	7825.2821	−5	–
A^-	B^-	B^+	$2_{1,1}$	←	A^+	A^+	A^+	$2_{0,2}$	10	7825.5789	27	–
B^+	A^+	B^+	$3_{1,2}$	←	B^-	B^-	A^+	$3_{0,3}$	6	7825.6051	−4	0.0207(35)
A^-	B^-	B^+	$4_{1,3}$	←	A^+	A^+	A^+	$4_{0,4}$	10	7825.6455	12	0.0219(16)
B^+	A^+	B^+	$5_{1,4}$	←	B^-	B^-	A^+	$5_{0,5}$	6	7825.6926	−2	0.0221(21)
A^-	B^-	B^+	$6_{1,5}$	←	A^+	A^+	A^+	$6_{0,6}$	10	7825.7487	−20	0.02589(68)
B^+	A^+	B^+	$7_{1,6}$	←	B^-	B^-	A^+	$7_{0,7}$	6	7825.8178	−3	0.0197(22)
A^-	B^-	B^+	$8_{1,7}$	←	A^+	A^+	A^+	$8_{0,8}$	10	7825.8949	0	0.01718(78)
B^+	A^+	B^+	$9_{1,8}$	←	B^-	B^-	A^+	$9_{0,9}$	6	7825.9827	16	0.0224(27)
A^-	B^-	B^+	$10_{1,9}$	←	A^+	A^+	A^+	$10_{0,10}$	10	7826.0770	4	0.0241(22)
B^+	A^+	B^+	$11_{1,10}$	←	B^-	B^-	A^+	$11_{0,11}$	6	7826.1790	−25	–
B^-	B^-	A^+	$5_{1,5}$	←	B^+	A^+	B^+	$4_{0,4}$	6	7826.2195	62	–
A^-	B^-	B^+	$12_{1,11}$	←	A^+	A^+	A^+	$12_{0,12}$	10	7826.2976	15	0.0146(11)
A^-	B^-	B^+	$14_{1,13}$	←	A^+	A^+	A^+	$14_{0,14}$	10	7826.5559	6	0.0203(22)
A^+	A^+	A^+	$6_{1,6}$	←	A^-	B^-	B^+	$5_{0,5}$	10	7826.6837	−47	0.0207(38)
A^-	B^-	B^+	$16_{1,15}$	←	A^+	A^+	A^+	$16_{0,16}$	10	7826.8566	−9	–
A^-	B^-	B^+	$3_{1,3}$	←	A^+	A^+	A^+	$2_{0,2}$	10	7826.8899	26	–
B^-	B^-	A^+	$7_{1,7}$	←	B^+	A^+	B^+	$6_{0,6}$	6	7827.1709	12	–
A^-	B^-	B^+	$18_{1,17}$	←	A^+	A^+	A^+	$18_{0,18}$	10	7827.2093	2	–
B^+	A^+	B^+	$4_{1,4}$	←	B^-	B^-	A^+	$3_{0,3}$	6	7827.3414	−58	–
A^+	A^+	A^+	$8_{1,8}$	←	A^-	B^-	B^+	$7_{0,7}$	10	7827.6563	−8	–
A^-	B^-	B^+	$5_{1,5}$	←	A^+	A^+	A^+	$4_{0,4}$	10	7827.8164	30	–

Table 7. Spectroscopic parameters of the $K_a=1$ level of the $N_j=2_3$ band of $(HF)_2$.[a)]

Parameter	$\Gamma_{vt}=A^+$	$\Gamma_{vt}=B^+$
$\tilde{\nu}$/cm^{-1}	7824.5977 (16)	7825.5469 (16)
$\Delta\tilde{\nu}_T$/cm^{-1}	0. 9492 (22)	
B/cm^{-1}	0. 221125 (98)	0. 220842 (71)
$D/10^{-6}$ cm^{-1}	5.0 (15)	2.99 (41)
$H/10^{-12}$ cm^{-1}	9900 (540)	2440 (830)
$b/10^{-3}$ cm^{-1}	3.277 (67)	3.03 (17)
$N_{data}=37$	$D_{RMS}=2.3\times10^{-3}$ cm^{-1}	

[a)] Values in parentheses represent one standard deviation in the units of the last digit quoted.

5. Mode-Selective Predissociation Dynamics

The dimer (HFHF) is weakly bound characterised by a hydrogen bond with a modest dissociation energy D_0 of about 12.7 kJ mol^{-1}.[8,76–78] HF-stretching excitation exceeds the dissociation threshold by far, and fast predissociation can thus be expected for all three vibrational levels with two quanta of HF-stretching excitation in the $N=2$ triad. The nature of vibrational excitation has apparently also a distinct influence on the predissociation dynamics of the $(HF)_2$ cluster: The longest predissociation lifetimes in the $N=2$ triad are found for the $N=2_2$ component, where the HF hydrogen-bond acceptor is excited with two quanta, $\tau_{PD}=1.09(15)$ ns for $\Gamma_{vt}=A^+$ and 1.80(29) ns for $\Gamma_{vt}=B^+$ in the $K_a=0$ level and 1.32(13) ns for $\Gamma_{vt}=A^+$ and 1.89(25) ns for B^+ sublevels in the $K_a=1$ level of $N=2_2$. In $N=2_3$, both HF units are excited with one quantum of HF-stretching excitation each. The predissociation lifetimes in this component are considerably shorter, $\tau_{PD}=320(70)$ ps for $\Gamma_{vt}=A^+$ and $\tau_{PD}=340(50)$ ps for $\Gamma_{vt}=B^+$ in the $K_a=0$ level, and $\tau_{PD}=240(50)$ ps for $\Gamma_{vt}=A^+$ and $\tau_{PD}=250(40)$ ps for $\Gamma_{vt}=B^+$ in the $K_a=1$ level of $N=2_3$. With $\tau_{PD}=51.2(56)$ ps for A^+ and 49(10) ps for B^+, the shortest predissociation lifetimes are in the $K_a=0$ level of $N=2_1$, where the HF hydrogen-bond donor is excited with two quanta. The more HF-stretching quanta are in the hydrogen-bond donor, the faster the predissociation of the dimer. This behaviour corresponds qualitatively to what one might expect intuitively: the more the vibration involved directly in the hydrogen bond is excited, the shorter the lifetime.

The present experimental results for the $N=2$ triad can also be compared with previous results for other polyads studied, $N=1$ and $N=3$ (see Table 8). With increasing vibrational excitation, predissociation becomes faster: with increasing number of HF-stretching quanta, the lifetime is decreasing, for example $\tau_{PD}=480$ ps in $N=1_1$, 50 ps in $N=2_1$ and 16 ps in $N=3_1$. Within a given polyad, the predissociation lifetime of the excitation of the donor mode with N stretching quanta is orders of magnitude shorter than the excitation of the acceptor mode with N stretching quanta. In vibrational states where both modes are excited, the lifetimes are between these extreme values. The lifetimes in the mixed excitation states $N_j=2_3$ and 3_4 are similar to the lifetime in the $N_j=1_1$ state; in all these states, the donor is excited with just one HF-stretching quantum, but the acceptor with 0 to 2 quanta, which shows again the greater influence of vibrational excitation of the donor mode compared to the acceptor mode. In all three polyads, no systematic trend for the dependence of the predissociation lifetime on K_a-excitation or on the tunneling sublevel is apparent.

The pronounced influence of donor mode excitation on the predissociation dynamics can be understood qualitatively with a simple consideration: in the equilibrium geometry of $(HF)_2$, the H–F bond of the donor molecule is nearly in line with the intermolecular hydrogen bond, whereas the H–F bond of the acceptor molecule is nearly perpendicular to it. In an HF-

Table 8. Predissociation lifetime of various vibrational states of $(HF)_2$. The states are characterized by the polyad quantum number N_j, the approximate local mode assignment, the tunneling level and the K_a rotational constant. The local mode assignment is given in terms of the hydrogen bond donor ν_{don} and acceptor mode ν_{acc}, which correspond to a stretching excitation of the hydrogen bonded and the free monomer respectively. Values in parentheses represent one standard deviation in the units of the last digit quoted.

	Approx.	τ_{PD}/ps			
N_j	Local	$\Gamma_{vt}=A^+$		$\Gamma_{vt}=B^+$	
	Mode	$K_a=0$	$K_a=1$	$K_a=0$	$K_a=1$
1_1 (Ref. [73])	ν_{don}	480(40)	–	480(40)	–
1_2 (Ref. [73])	ν_{acc}	16800(900)	13500(600)	24900(1900)	15600(800)
2_1 (Ref. [38])	$2\nu_{don}$	51(6)	–	49(10)	–
2_2 (Ref. [38])	$2\nu_{acc}$	–	1320(130)	–	1890(250)
2_2 (Ref. [43])	$2\nu_{acc}$	910(130)	1400(130)	2800(1000)	2380(280)
2_2 (this work)	$2\nu_{acc}$	1090(150)	–	1800(290)	–
2_3 (this work)	$\nu_{acc}+\nu_{don}$	320(70)	240(50)	340(50)	250(40)
3_1 (Ref. [74])	$3\nu_{don}$	16	–	16	–
3_2 (Ref. [74])	$3\nu_{acc}$	1590	84	1590	84
3_4 (Ref. [75])	$2\nu_{acc}+\nu_{don}$	200	–	200	–
4_2 (Ref. [79])	$4\nu_{acc}$ (?)			470 (30)	

stretching excitation of the donor molecule, the H-atom moves in the direction of the weak hydrogen bond, whereas in an excitation of the acceptor molecule, the hydrogen bond is not affected that much. It is thus not very surprising that predissociation is enhanced by excitation of the donor molecule compared to a corresponding excitation of the acceptor (see also the early work of Halberstadt *et al.*, Ref. [80]). This simple picture, however, is not sufficient for explaining the time scale and details of the predissociation process, for example the dependence on K_a excitation or on the tunneling sublevel. The HF-stretching vibration has a period of about 8 to 9 fs, only, and many oscillations will thus occur in any case until the dimer dissociates. Vibrational energy redistribution from the HF-stretching vibration into the weak hydrogen bond thus governs the predissociation dynamics in the HF-dimer, and a full description of the dynamics has to take into account the coupling of intra- and intermolecular vibrational modes.

An interesting question would be whether classical molecular dynamics simulations (MD) or full-dimensional quantum dynamics can describe the trends in vibrational predissociation qualitatively and quantitatively. This was investigated in some detail in Ref. [7] where classical MD simulations were compared to full quantum dynamics from the literature.[30,81,82] It turns out that while qualitative trends for predissociation rates as a function of HF stretching excitation in the initial state (also with donor and acceptor excitation) can be described by classical MD simulation, the quantitative results are quite inadequate. Also, when comparing classical MD with full quantum dynamical results on the same potential hypersurface (SQS BDE from Ref. [19] in this case), one finds large differences of a factor of about 3. Thus quantum effects are very important even though predissociation involves the motion of the 'heavy atom' framework by increasing the F···F distance in essence. One must say, however, that large differences are also observed when carrying out the calculations on somewhat different potential hypersurfaces (e.g., SQS BDE vs SO-3 from Ref. [8]). While this result might be expected, it must be kept in mind.

6. Tunneling Dynamics of the Hydrogen-Bond Switching Process

During the hydrogen bond switching process, both HF monomers exchange their function in the dimer: the hydrogen bonded monomer (donor) becomes the free monomer (acceptor), and *vice versa* (see Figure 2). This tunneling process has an electronic barrier of about 4.2 kJ mol^{-1}; it results in an observable spectroscopic tunneling splitting $\Delta\nu_T$, from which the tunneling period τ_T can be determined (Equ. 3). In Figure 7 the symmetry structure of the lower polyads including the signed tunneling splittings is shown, where the symmetry ordering corresponds to the present experimental results and to our variational calculations on the SO-3 hypersurface. HF stretching excitations can be considered as related to symmetry in the permutation inversion group M_{S4}, if we take the lower HF stretching vibration to be of symmetric (A) and the upper to be antisymmetric (B) symmetry species in M_{S4}. The

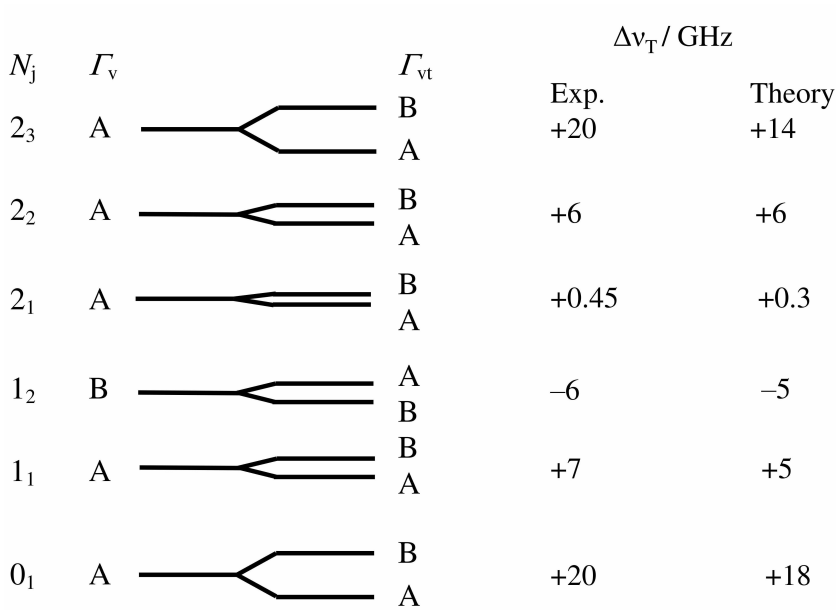

Figure 7. Symmetry structure, mode selective tunneling rearrangement and energy transfer in the polyads, $N=0$, 1, and 2. The levels are characterized by their polyad quantum number N including the level numbering within the polyad as index j, the 'empirical' vibrational symmetry Γ_v for each level, and the tunneling-vibrational symmetry Γ_{vt} for each sublevel. Refs. for experimental and calculated (on SO-3) tunneling splittings are provided in Table 9.

tunneling splitting is normal (positive) in the vibrational ground state and in the symmetric HF-stretching vibration $N=1_1$, where the A level is lower in energy. In the antisymmetric HF-stretching vibration $N=1_2$, the splitting is inverted (negative), with the antisymmetric B level being lower in energy than the symmetric A tunneling sublevel. Indeed, in a simple picture assigning total vibrational-tunneling symmetry as a product of vibrational and of tunneling symmetry, one expects such inverted splittings for all polyad levels with an odd number of quanta in the antisymmetric normal mode. However, whether such a simple symmetry assignment is adequate must be checked by experiment, which is the reason to mark it with a question mark in Figure 1 for the $N=2$ polyad.

The $N=2$ polyad (the first HF stretching overtone) consists of three components corresponding to the different possibilities to distribute two HF stretching quanta among the HF-monomer units and one expects from such a simple picture one inverted tunneling sublevel system. In this sense one can also take the assignment of tunneling sublevel symmetry as an assignment of vibrational level symmetry. In this polyad, our variational calculations[32,33] on the SO-3 hypersurface predict, however, the tunneling splittings in all three components to be normal, in agreement with our experiment, whereas previous calculations[83,84] on different hypersurfaces predicted two components to have normal and one component to have an inverted splitting. There has been an extensive debate in the literature using a variety of different simplified quantum dynamical models and also quantum calculations on different full-dimensional potential hypersurfaces (Refs. [35, 58–65, 85], see also [86–88]). While we shall not attempt here to review this debate in any detail, we can summarize that while the different simplified models provide different magnitudes for the tunneling and also different ordering of the tunneling sublevels, they all predict one level with antisymmetric (B) vibrational symmetry in the $N=2$ polyad. The full quantum calculations sometimes predict one antisymmetric vibrational B-level and sometimes, with a different surface, they predict 3 symmetric (A) vibrational levels.

The present experimental results allow the resolution of this debate: The experimental tunneling splitting is 0.45 GHz for the $K_a=0$ level of the $N=2_1$ component. For the $N=2_2$ component, 6.468 GHz and 2.808 GHz are obtained for the $K_a=0$ and $K_a=1$ levels, respectively. The experimental splittings for the $N=2_3$ component are 20.283 GHz and 14.19 GHz for the $K_a=0$ and $K_a=1$ levels, respectively. In all three components, the experimentally determined sign is thus positive, and tunneling splitting in these components is normal. This is in agreement with our calculations for $K_a=0$ on the SO-3 hypersurface, 0.27 GHz for $N=2_1$, 6.21 GHz for $N=2_2$ and 14.19 GHz for $N=2_3$, both with respect to sign and magnitude.[33] The long-standing discussion about the sign of the tunneling splitting is thus resolved by our experiments in favor of the SO-3 surface results and is in opposition to the whole variety of simple quantum dynamical models.

Hydrogen bond switching is much faster in the $N=2_3$ component compared to $N=2_1$ or $N=2_2$. This may be explained qualitatively by a simple model: A coordinated rotation of both monomer units changes the equilibrium geometry where one monomer is the hydrogen bond acceptor and the other the donor, into the equivalent geometry where the acceptor/donor function has been exchanged. For $N=2_1$ or $N=2_2$, vibrational excitation has in addition to be redistributed from the one monomer unit with two quanta of HF-stretching vibration to the other monomer in order to obtain an equivalent situation including at the same time a change in the vibrationally averaged HF bond lengths. This hinders the hydrogen bond switching process in these two components, hence the small tunneling splittings. In $N=2_3$, both HF-monomer units are excited by one quantum of HF-stretching vibration. In this case, redistribution of vibrational excitation and average bond length has to occur to a lesser extent in the hydrogen bond switching process in order to obtain an equivalent situation, and thus the tunneling splitting is much larger. While this picture is obviously highly simplified, it provides some intuitive insight.

An alternative intuitive picture uses an adiabatic separation of the high frequency modes from the low frequency tunneling motion. Here the change of tunneling splittings with various degrees of HF stretching excitation arises (i) from a change in the effective quasi-adiabatic barrier for the tunneling motion, and (ii) from a change of the 'effective tunneling mass' (really an 'effective tunneling moment of inertia' for the internal rotation type motion) which arises from the lengthening of the average HF bond lengths with the stretching excitation. This picture can be made the basis of quantitative approximations either using the quasi-adiabatic channel Quantum Monte Carlo method[9,19] or with $(4+2)$ dimensional calculations on effective 4-dimensional hypersurfaces for the tunneling motion which are different for different combinations (v_1, v_2) of the HF stretching excitation. Indeed, quasi-adiabatic channel reaction path Hamiltonian treatments have been quite successful for stereomutation tunneling in hydrogen peroxide HOOH, for example, or for the inversion tunneling in aniline.[47,89–92] We may mention also the relation of this concept to the statistical adiabatic channel model (SACM).[93] However, quantitatively accurate predictions are rather to be expected from full-dimensional calculations on adequate potential hypersurfaces, which proved necessary for describing inversion in ammonia isotopomers.[94]

We should add here a more fundamental remark. In full-dimensional calculations on a 6-dimensional Born-Oppenheimer (or related) electronic potential hypersurface, the 'tunneling splittings' arise, although one has dynamics high above the modest tunneling barrier, in fact even high above the dissociation limit in the present example. In a quasi-adiabatic channel picture one can understand the tunneling spectra qualitatively as tunneling through an effective vibrationally quasi-adiabatic barrier (see Figure 2). Such a simple understanding is not possible on the full-dimensional potential hypersurface. Indeed, one can even go beyond the Born-

Oppenheimer approximation and use a Coulombic potential hypersurface (in a very high-dimensional space treating all electrons and nuclei as particles of the model). Finally, one could even go beyond this description and treat the dynamical problem using elementary particles and the four fundamental forces with their field particles, in the framework of the SMPP (standard model of particle physics). In none of these much more fundamental descriptions one has simply tunneling through some barrier. Nevertheless, theoretical 'tunneling spectra' and splittings arise as also in the experimental spectra. As we have discussed elsewhere, at the most fundamental level tunneling spectral structures arise from approximate symmetries in the underlying dynamics and their successive breaking and similar considerations apply to spectral structures described by predissociation line widths (see Refs. [10, 95]).

The present experimental tunneling splittings and available previous results for the $N=0$, 1 and 2 polyads are shown in the graphical overview of Figure 7 and are listed in Table 9, compared with our calculations on the SO-3 hypersurface and further results for low frequency excitation. For all polyads we find a reasonable agreement between experimental results and calculations, with the calculated splittings slightly below the experimental values. The sign of the tunneling splitting is reproduced in all cases, where experimental data are available. We might note here that following the early measurements which did not allow for analyses in the $N=3$ and 4 polyads[6] more recently there has been a partial assignment of components in these polyads, which does, however, not yet allow for a complete survey of the symmetry assignments of all the levels.[79] A band at 14700.5 cm^{-1} was assigned to an isolated level as (4,0) or the member 4_2 of $N=4$ polyad, in agreement with calculations on the SO-3 surface.[8] However, the tunneling splitting was found to be quenched and the difference between A and B sublevels smaller than the uncertainty in the position, and thus no definitive symmetry assignment was possible (Ref. [79], see also the discussion in Refs. [63, 74, 75]).

7. Discussion and Conclusions

As can be seen from the surveys in Figure 7 and Table 9, the assignment of the HF stretching polyad spectra in (HFHF) is now complete up to the polyad $N=2$ involving various combinations of HF stretching excitation. The assignment is firm, given the good agreement with predictions from the best currently available potential hypersurface (SO-3 from [8, 33, 42, 50]) and the qualitative intensity patterns as well as detailed line by line symmetry and nuclear spin statistical weight assignments. Alternative assignments to various possible combination levels *etc.* can essentially be excluded. Perhaps the most surprising result concerns the symmetry ordering, which confirms three polyad levels with a formal vibrational A-symmetry, as defined through unambiguous 'normal' tunneling sublevel ordering with a lower 'symmetric' level of A symmetry in M_{S4} and an upper 'antisymmetric' level

Table 9. Survey of selected experimental and calculated energy levels ν_i and N_J, and tunneling splittings Δ_i ($K_a=0$) (values given in cm^{-1}).

Level	Exp.	Calc. SO-3 [a]	Calc. HYZX [b]	Calc. RPB [c]	Refs. (Exp.)
Δ_0	0.65869	0.59 (0.63) [d]	0.665	0.677	[18, 55, 96, 97]
ν_4	125	126.6	125.3	127.66 (126.8)	[19]
Δ_4	>2 (3.15)	3.13	2.98 (2.95)	3.14 (2.95)	[19]
ν_5	161	162.9	162.4	166.02 (165.5)	[20]
Δ_5	?	7.19	7.88	7.65	
ν_6	417.505	420.83	413.271	418.6 (418.4)	[21, 98]
Δ_6	2.209	2.22	2.284	2.13	[21, 98]
ν_3	486.944	483.48	481.647	490.5 (484.4)	[98]
Δ_3	−0.061	2.65	−0.325	1.21	[98]
1_1	3868.079	3867.09	3871.874		[23, 24]
$\Delta(1_1)$	0.233	0.18	0.232		
1_2	3930.903	3929.17	3931.803		[23, 24]
$\Delta(1_2)$	−0.215	−0.17	−0.225		[23, 24]
2_1	7550.336	7550 [e] (7543)			[38] ([42]) [e]
$\Delta(2_1)$	0.015	0.02 (0.0009)			[38] ([42])
2_2	7682.818	7679.8			this work, [6,43]
$\Delta(2_2)$	0.216	0.207			this work, [6, 38, 42, 43, 50]
2_3	7795.255	7793.92			this work
$\Delta(2_3)$	0.676	0.473			this work
D_0	1062	1062 (1061.73)	1037.51	1065.62	[76, 78] ([8, 28, 36]) [e]

[a] Calculations on the SO-3 surface are from this work (see also [32, 33, 42, 85, 88], with differing results in parentheses); [b] Ref. [36], [c] Ref. [41], values taken from the supplementary tables, the values in parentheses from the respective columns Pall in the tables of [41], including all corrections by calculating $\tilde{\nu}_{calc} = \tilde{\nu}_{obs} - Pall$; [d] 4+2 D result from [8, 99]; [e] see also references to theory therein (thus the parentheses).

of B symmetry. While this appears to contradict intuition and all simple models proposed during a long debate in the past (see Refs. [58–64], for example), it is in fact perfectly possible and in agreement with a sufficiently advanced theory.[8] When considering the seemingly counter-intuitive symmetry picture for the tunneling sublevels, one must realize that effective one-dimensional separable tunneling models are often inadequate and the multi-dimensional nature of tunneling can result in a change of tunneling sublevel positions as compared to simple models quite easily, as the energies needed in such interactions are actually small when the tunneling splittings are small.[10,94] The results on rearrangement tunneling times on the pico-second to nanosecond time scales show highly mode selective behaviour as it is observed also in other types of rearrangement tunneling, such as tunneling stereomutation[10,47,89–92]. In agreement with the earliest results on the $N=1$ and $N=2$ polyads,[3,4,6,23,24] HF stretching in general acts as an inhibiting mode for rearrangement tunneling, in qualitative agreement with a vibrationally quasi-adiabatic channel picture for the dynamics; tunneling splittings in the excited HF-stretching states are smaller and corresponding tunneling times longer than in the ground state. Only in the 2_3 polyad level tunneling rearrangement is similar to the ground state, which again has a qualitative interpretation, as this level corresponds to equal excitation of each HF unit with one quantum, thus removing an essential part of the inhibiting effect of stretching excitation. The long story of the interplay of HF stretching and rearrangement tunneling has thus been completed up to the $N=2$ polyad by now. The continuation for the higher polyads $N=3$ and $N=4$ has been started as well by early measurements long ago,[6] but so far assignments are still incomplete with only 3 out of 4 sublevels being observed and analyzed for $N=3$ (and in part uncertain assignment [63, 74, 75]) and only one member out of 5 for $N=4$ (Ref. [79]).

Another aspect of our larger project of investigating the high resolution spectra of $(HF)_2$ from the far infrared to the visible range was to provide an experimental benchmark for the *ab initio* theory of this prototypical hydrogen bonded system, which has, indeed, been studied from the early days of quantitative, accurate electronic structure theory (Refs. [39, 40] and refs therein and in Ref. [100]), including also repeated efforts in designing full dimensional potential hypersurfaces (Refs. [8, 19, 25, 36] and refs cited therein and in reviews [100, 101], see also [102, 103]) and quantum dynamics calculations (see Refs. [19, 29–37, 42, 52–54, 77, 81–83, 104, 105] and refs cited therein and in Ref. [65]). Table 9 includes also experimental and theoretical work on the four low frequency ′intermolecular′ modes in this context. As can be seen, most low frequency modes act as promoting modes for rearrangement tunneling, the tunneling splittings increasing with vibrational excitation of all the low frequency modes, with the exception of ν_3, where also the agreement between experiment and theory is not so good. For ν_5, the tunneling spectra remain to be analysed in order to complete the available information.

Table 9 also contains the dissociation energy D_0 as important information and for this quantity a very accurate recent *ab initio* calculation provided $D_0=(1036.7\pm35)\ cm^{-1}$ including estimates of systematic errors arising from the zero point energy calculation.[106] When looking at the overall picture comparing experiment and theory, the three best current potential hypersurfaces SO-3 (Ref. [8]), HYZX (Ref. [36]) and RPB (Ref. [41]) perform about similarly well, with a slight advantage for the empirically optimized SO-3 surface, particularly when also taking D_0 as an important property (for HYZX there remains also a gap on the theory for the $N=2$ polyad, and for RPB,[41] no excited HF stretching results have been reported, so far).

Further important results pertain to the vibrational predissociation kinetics summarized in Table 8. In agreement with the early experimental results the unimolecular hydrogen bond dissociation of $(HF)_2$ is highly nonstatistical, mode selective[3,4,6,23,24] and much slower than predicted by statistical theories such as RRKM or microcanonical transition state theory.[6] As reviewed in Ref. [7], full dimensional quantum theory for predissociation can be quite successful quantitatively, whereas classical molecular dynamics can provide some qualitative trends but fails quantitatively. On the other hand, the simple intuitive picture that excitation of the HF stretching vibration directly involved in the hydrogen bond (i.e., ν_{don}) promotes dissociation, whereas exciting the ′spectator′ vibration (i.e., ν_{acc}) is rather ineffective, is perfectly well demonstrated by the three sublevels of the $N=2$ polyad (Table 8).

The highly nonstatistical nature of hydrogen bond dissociation in (HFHF) cluster is obviously related to a strong, nonstatistical inhibition of intramolecular vibrational energy flow as one of the increasing number of examples of the nonstatistical nature of intramolecular vibrational redistribution in polyatomic systems (see Refs. [47, 107–111], for example, and refs cited therein). However, the infrared multiphoton excitation of the large, covalently bound cluster C_{60} leading to the early observation of vibrational preionization to give rise to the ionic cluster C_{60}^+ and its further fragmentation appeared to be largely statistical.[112] Followed by many studies also of the spectra and fragmentation of ionic clusters[113] it remains to be seen where and how the transition between statistical and nonstatistical fragmentation of ionic clusters occurs and can be understood.[1,2,113] Related questions arise as well in the study of energy transfer and desorption of small molecules adsorbed on surfaces.[114]

Going beyond the particularly simple prototypical system (HFHF) one can also try to draw some qualitative conclusions of similar kind for the kinetic primary processes of hydrogen bond dissociation and rearrangement in larger cluster $(HF)_{n>2}$, other types of hydrogen bonded clusters such as $(H_2O)_n$ (Ref. [115]) and hydrogen bonded liquids and crystals. Such kinetic primary processes occur also in biomolecular hydrogen bonded systems, DNA and proteins[14–17,116–118] and results on the simplest prototypical hydrogen bond may stimulate even models for drug design and enzymes.[119,120]

Acknowledgements

We are grateful to Katharina Al-Shamery (née v. Puttkamer), Jochen Blumberger, Yabei He, Hans Hollenstein, David Luckhaus, Carine Manca Tanner, Frédéric Merkt, Holger Müller, Georg Seyfang, Ruth Signorell, Martin Suhm and Gunther Wichmann for help and discussions at various stages of our work, and Z. Bačić for correspondence and discussions in an extended collaboration on the theory of $(HF)_2$, the results of which will be published elsewhere. Our work is supported financially by the ETH Zürich, the Schweizerischer Nationalfonds and the AGS project, as well as COST MOLIM and COST COSY and an Advanced Grant from the ERC. Michael Hippler acknowledges support by a visiting professorship at ETH Zürich. We are also grateful for the helpful comments by the reviewers of our manuscript.

Data Availability Statement

The data that support the findings of this study are available from the corresponding author upon reasonable request.

References

[1] G. Depke, C. Lifshitz, H. Schwarz, E. Tzidony, *Angew. Chem. Int. Ed. Engl.* **1981**, *20*, 792–793.
[2] M. Quack, *Il Nuovo Cimento* **1981**, *63B*, 358–377.
[3] K. v Puttkamer, M. Quack, *Chimia* **1985**, *39*, 358–360.
[4] a) K. v. Puttkamer, M. Quack, *Faraday Discuss. Chem. Soc.* **1986**, *82*, 377–381; b) K. v. Puttkamer, M. Quack, *Proceedings COMET X – 10th International conference on molecular energy transfer*, P. Dietrich, M. Quack (Eds), pp 195–197, Laboratory for Physical Chemistry, Zürich, **1987**.
[5] K. Tanaka, K. Harada, K. M. T. Yamada, *THz and Submillimeter-wave Spectroscopy of Molecular Complexes, in Handbook of High Resolution Spectroscopy*, Vol. 2, M. Quack, F. Merkt (Eds), pp 854–896, Wiley, Chichester New York, **2011**.
[6] K. v Puttkamer, M. Quack, *Chem. Phys.* **1989**, *139*, 31–53.
[7] C. Manca, M. Quack, M. Willeke, *Chimia* **2008**, *62*, 235–239.
[8] W. Klopper, M. Quack, M. A. Suhm, *J. Chem. Phys.* **1998**, *108*, 10096–10115.
[9] M. Quack, M. A. Suhm, *Chem. Phys. Lett.* **1991**, *183*, 187–194.
[10] M. Quack, G. Seyfang, *Atomic and Molecular Tunnelling Processes in Chemistry, Chapter 7 in Molecular Spectroscopy and Quantum Dynamics*, R. Marquardt, M. Quack (Eds), pp 231–282, Elsevier, Amsterdam, **2021**.
[11] M. Eigen, *Angew. Chem.* **1963**, *75*, 489–508.
[12] P. Schuster (Ed.), *Topics in Current Chemistry* Vol. 120, *Hydrogen Bonds*, Springer, Berlin **1984**.
[13] N. Sheppard, *Hydrogen Bonding*, D. Hadzi (Ed.), p. 85, Pergamon Press, New York, **1985**.
[14] C. B. Aakeröy, K. R. Seddon, *Chem. Soc. Rev.* **1993**, *22*, 397–407.
[15] S. Scheiner, *Hydrogen Bonding*, Oxford University Press, New York, **1997**.
[16] G. R. Desiraju, T. Steiner, *The Weak Hydrogen Bond*, Oxford University Press, Oxford, **1999**.
[17] M. Hippler, *Phys. Chem. Chem. Phys.* **2002**, *4*, 1457–1463.
[18] T. R. Dyke, B. J. Howard, W. Klemperer, *J. Chem. Phys.* **1972**, *56*, 2442–2454.
[19] M. Quack, M. A. Suhm, *J. Chem. Phys.* **1991**, *95*, 28–59.
[20] M. Quack, M. A. Suhm, *Chem. Phys. Lett.* **1990**, *171*, 517–524.
[21] K. v Puttkamer, M. Quack, *Mol. Phys.* **1987**, *62*, 1047–1064.
[22] K. v Puttkamer, M. Quack, M. A. Suhm, *Infrared Phys.* **1989**, *29*, 535–539; K. v Puttkamer, M. Quack, M. A. Suhm, *Mol. Phys.* **1988**, *65*, 1025–1045.
[23] A. S. Pine, W. J. Lafferty, *J. Chem. Phys.* **1983**, *78*, 2154–2162.
[24] A. S. Pine, W. J. Lafferty, B. J. Howard, *J. Chem. Phys.* **1984**, *81*, 2939–2950.
[25] M. Kofranek, H. Lischka, A. Karpfen, *Chem. Phys.* **1988**, *121*, 137–153.
[26] P. R. Bunker, T. Carrington Jr, P. C. Gomez, M. D. Marshall, M. Kofranek, H. Lischka, A. Karpfen, *J. Chem. Phys.* **1989**, *91*, 5154–5159.
[27] M. Quack, M. A. Suhm, *Mol. Phys.* **1990**, *69*, 791–801.
[28] W. Klopper, M. Quack, M. A. Suhm, *Chem. Phys. Lett.* **1996**, *261*, 35–44.
[29] D. H. Zhang, Q. Wu, J. Z. H. Zhang, *J. Chem. Phys.* **1995**, *102*, 124–132.
[30] D. H. Zhang, Q. Wu, J. Z. H. Zhang, M. v Dirke, Z. Bačić, *J. Chem. Phys.* **1995**, *102*, 2315–2325.
[31] W. C. Necoechea, D. G. Truhlar, *Chem. Phys. Lett.* **1996**, *248*, 182–188.
[32] Z. Bačić, Y. Qiu, J. Z. H. Zhang, H. B. Müller, M. Quack, to be published.
[33] J. Blumberger, L. Oeltjen, M. Quack, Z. Bačić, Y. Qiu, J. Z. H. Zhang, *Faraday Discuss.* **2001**, *118*, 431; and in preparation.
[34] H. Sun, R. O. Watts, *J. Chem. Phys.* **1990**, *92*, 603–616.
[35] M. Quack, M. A. Suhm, *Chem. Phys. Lett.* **1995**, *234*, 71–76.
[36] J. Huang, D. Yang, Y. Zhou, D. Xie, *J. Chem. Phys.* **2019**, *150*, 154302.
[37] O. Polyansky, R. I. Ovsyannikov, J. Tennyson, S. P. Belov, M. Yu Tretyakov, V. Yu Makhnev, N. F. Zobov, *J. Mol. Spectrosc.* **2021**, *379*, 111481.
[38] M. Hippler, L. Oeltjen, M. Quack, *J. Phys. Chem. A* **2007**, *111*, 12659–12668; M. Hippler, L. Oeltjen, M. Quack, *Chimia* **2001**, *55*, 654 (contr. 271).
[39] D. R. Yarkony, S. V. O'Neil, H. F. Schaefer, III, C. P. Baskin, C. F. Bender, *J. Chem. Phys.* **1974**, *60*, 855–865.
[40] C. L. Collins, K. Morihashi, Y. Yamaguchi, H. F. Schaefer, III, *J. Chem. Phys.* **1995**, *103*, 6051–6056.
[41] R. I. Ovsyannikov, V. Yu Makhnev, N. F. Zobov, J. Koput, J. Tennyson, O. L. Polyansky, *J. Chem. Phys.* **2022**, *156*, 164305.
[42] Y. He, H. B. Müller, M. Quack, M. A. Suhm, *Z. Physik. Chem.* **2007**, *221*, 1581–1645.
[43] M. A. Suhm, J. T. Farrell Jr, A. McIlroy, D. J. Nesbitt, *J. Chem. Phys.* **1992**, *97*, 5341–5354.
[44] Y. He, M. Hippler, M. Quack, *Chem. Phys. Lett.* **1998**, *289*, 527–534.
[45] M. Hippler, M. Quack, *Chem. Phys. Lett.* **1999**, *314*, 273–281.
[46] M. Hippler, M. Quack, *J. Chem. Phys.* **2002**, *116*, 6045–6055.
[47] M. Hippler, E. Miloglyadov, M. Quack, G. Seyfang, *Mass and Isotope selective infrared spectroscopy, in Handbook of High Resolution Spectroscopy*, Vol. 2, M. Quack, F. Merkt (Eds), pp 1069–1118, Wiley, Chichester, New York, **2011**.
[48] C. M. Lovejoy, D. J. Nesbitt, *Rev. Sci. Instrum.* **1987**, *58*, 807–811.
[49] H. Hollenstein, M. Quack, E. Richard, *Chem. Phys. Lett.* **1994**, *222*, 176–184.
[50] R. Signorell, Y. He, H. B. Müller, M. Quack, M. A. Suhm, in J. P. Maier, M. Quack (Eds), *Proceedings of the 10th Interna-*

tional Symposium on Atomic, Molecular, Cluster, Ion and Surface Physics SASP 96, pp. 256–259, VdF Publishers Zürich, **1996**.
[51] C. M. Lovejoy, D. J. Nesbitt, *J. Chem. Phys.* **1989**, *90*, 4671–4680.
[52] Z. Bačić, J. C. Light, *Annu. Rev. Phys. Chem.* **1989**, *40*, 469–498.
[53] Z. Bačić, J. C. Light, *J. Chem. Phys.* **1986**, *85*, 4594–4604.
[54] Z. Bačić, J. C. Light, *J. Chem. Phys.* **1987**, *86*, 3065–3077.
[55] M. Quack, M. A. Suhm, *Chem. Phys. Lett.* **1991**, *183*, 187–194.
[56] M. Quack, *Mol. Phys.* **1977**, *34*, 477–504.
[57] M. Quack, *Fundamental Symmetries and Symmetry Violations from High Resolution Spectroscopy, in Handbook of High Resolution Spectroscopy*, Vol. 1, M. Quack, F. Merkt (Eds), pp 659–722, Wiley, Chichester, New York, **2011**.
[58] I. M. Mills, *J. Phys. Chem.* **1984**, *88*, 532–536.
[59] J. T. Hougen, N. Ohashi, *J. Mol. Spectrosc.* **1985**, *109*, 134–165.
[60] E. L. Sibert, III, *J. Phys. Chem.* **1989**, *93*, 5022–5024.
[61] G. C. Hancock, D. G. Truhlar, *J. Chem. Phys.* **1989**, *90*, 3498–3505.
[62] G. T. Fraser, *J. Chem. Phys.* **1989**, *90*, 2097–2108.
[63] H.-C. Chang, W. Klemperer, *J. Chem. Phys.* **1996**, *104*, 7830–7835.
[64] M. D. Schuder, D. D. Nelson, D. J. Nesbitt, *J. Chem. Phys.* **1993**, *99*, 5045–5060.
[65] M. Quack, M. A. Suhm, in *Advances in Molecular Vibrations and Collision Dynamics, Vol. III, Molecular Clusters*, Z. Bačić, J. Bowman (Eds), 205–248, JAI Press, Stamford, Conn. and London, England, **1998**.
[66] F. Merkt, M. Quack, Chapter 1 in *Handbook of High Resolution Spectroscopy*, Vol. 1, pp 1–55, Wiley, Chichester New York, **2011**.
[67] M. Snels, V. Horká-Zelenková, H. Hollenstein, M. Quack, *High-Resolution FTIR and Diode Laser Spectroscopy of Supersonic Jets, in Handbook of High Resolution Spectroscopy*, Vol. 2, M. Quack, F. Merkt (Eds), pp 1021–1067, Wiley, Chichester New York, **2011**.
[68] C. Manca Tanner, M. Quack, *Mol. Phys.* **2012**, *110*, 2111–2135.
[69] P. Dietiker, E. Miloglyadov, M. Quack, A. Schneider, G. Seyfang, *J. Chem. Phys.* **2015**, *143*, 244305.
[70] C. Manca Tanner, M. Quack, D. Schmidiger, *Mol. Phys.* **2018**, *116*, 3718–3730.
[71] V. Horká-Zelenková, G. Seyfang, P. Dietiker, M. Quack, *J. Phys. Chem. A* **2019**, *123*, 6160–6174.
[72] G. Wichmann, E. Miloglyadov, G. Seyfang, M. Quack, *Mol. Phys.* **2020**, *118*, e1752946.
[73] A. S. Pine, G. T. Fraser, *J. Chem. Phys.* **1988**, *89*, 6636–6643.
[74] H.-C. Chang, W. Klemperer, *J. Chem. Phys.* **1993**, *98*, 9266–9278.
[75] H.-C. Chang, W. Klemperer, *J. Chem. Phys.* **1994**, *100*, 1–14.
[76] R. E. Miller, *Acc. Chem. Res.* **1990**, *23*, 10–16.
[77] M. Mladenović, M. Lewerenz, *Chem. Phys. Lett.* **2000**, *321*, 135–141.
[78] E. J. Bohac, M. D. Marshall, R. E. Miller, *J. Chem. Phys.* **1992**, *96*, 6681–6695.
[79] Z. Yu, E. Hammam, W. Klemperer, *J. Chem. Phys.* **2005**, *122*, 194318.
[80] N. Halberstadt, P. Bréchignac, J. A. Beswick, M. Shapiro, *J. Chem. Phys.* **1986**, *84*, 170–175.
[81] D. H. Zhang, J. Z. H. Zhang, *J. Chem. Phys.* **1993**, *98*, 5978–5981.
[82] M. von Dirke, Z. Bačić, D. H. Zhang, J. Z. H. Zhang, *J. Chem. Phys.* **1995**, *102*, 4382–4389.
[83] Q. Wu, D. H. Zhang, J. Z. H. Zhang, *J. Chem. Phys.* **1995**, *103*, 2548–2554.
[84] P. Jensen, P. R. Bunker, A. Karpfen, M. Kofranek, H. Lischka, *J. Chem. Phys.* **1990**, *93*, 6266–6280.
[85] P. E. S. Wormer, A. van der Avoird, *Chem. Rev.* **2000**, *100*, 4109–4144.
[86] P. M. Felker, Z. Bačić, *J. Chem. Phys.* **2019**, *151*, 024305.
[87] P. M. Felker, Z. Bačić, *Phys. Chem. Chem. Phys.* **2022**, *24*, 24655–24676.
[88] G. W. M. Vissers, G. C. Groenenboom, A. van der Avoird, *J. Chem. Phys.* **2003**, *119*, 277–285 and 286–292.
[89] B. Fehrensen, D. Luckhaus, M. Quack, *Chem. Phys. Lett.* **1999**, *300*, 312–320.
[90] B. Fehrensen, D. Luckhaus, M. Quack, *Chem. Phys.* **2007**, *338*, 90–105.
[91] B. Fehrensen, M. Hippler, M. Quack, *Chem. Phys. Lett.* **1998**, *298*, 320–328.
[92] B. Fehrensen, D. Luckhaus, M. Quack, *Z. Phys. Chem.* **1999**, *209*, 1–19.
[93] M. Quack, J. Troe, *Statistical Adiabatic Channel Models, in Encyclopedia of Computational Chemistry*, Vol. 3 pp. 1775–1791, P. von Ragué Schleyer, N. L. Allinger, T. Clark, J. Gasteiger, P. A. Kollmann, H. F. Schaefer, III, P. R. Schreiner (Eds), John Wiley & Sons, Chichester, UK, **1998**.
[94] C. Fábri, R. Marquardt, A. G. Császár, M. Quack, *J. Chem. Phys.* **2019**, *150*, 014102.
[95] M. Quack, *Bunsen-Magazin* **2022**, *24*, 238–246.
[96] W. J. Lafferty, R. D. Suenram, F. J. Lovas, *J. Mol. Spectrosc.* **1987**, *123*, 434–452.
[97] S. P. Belov, E. N. Karyakin, I. N. Kozin, A. F. Krupnov, O. L. Polyansky, M. Yu Tretyakov, N. F. Zobov, R. D. Suenram, W. J. Lafferty, *J. Mol. Spectrosc.* **1990**, *141*, 204–222.
[98] H. Hollenstein, M. Quack (unpublished results); H. Hollenstein, M. Hippler, G. Seyfang, M. Quack (in preparation).
[99] D. Luckhaus, R. Meyer, M. Quack, M. A. Suhm (unpublished results); D. Luckhaus, H. B. Müller, M. Quack, M. A. Suhm, unpublished results cited in [42].
[100] M. Quack, M. A. Suhm, *Potential energy hypersurfaces for hydrogen bonded clusters $(HF)_n$, in Conceptual Perspectives in Quantum Chemistry*, E. S. Kryachko, J. L. Calais (Eds), pp 415–463, Kluwer, Dordrecht, 1997.
[101] R. Marquardt, M. Quack, *Global Analytical Potential Energy Surfaces for High Resolution Spectroscopy and Reaction Dynamics, Chapter 12 in Handbook of High Resolution Spectroscopy*, Vol. 1, M. Quack, F. Merkt (Eds), pp 511–549, Wiley, Chichester New York, **2011**.
[102] M. Quack, J. Stohner, M. A. Suhm, *J. Mol. Struct.* **2001**, *599*, 381–425.
[103] M. Quack, J. Stohner, M. A. Suhm, *J. Mol. Struct.* **1993**, *294*, 33–36.
[104] P. M. Felker, Z. Bačić, *J. Chem. Phys.* **2023**, *158*, 234109.
[105] Y. Volobuev, W. C. Necoechea, D. G. Truhlar, *Chem. Phys. Lett.* **2000**, *330*, 471–474.
[106] J. Řezáč, P. Hobza, *J. Chem. Theory Comput.* **2014**, *10*, 3066–3073.
[107] M. Quack, J. Stohner, *J. Phys. Chem.* **1993**, *97*, 12574–12590.
[108] M. Quack, *J. Mol. Struct.* **1993**, *292*, 171–195.
[109] R. Marquardt, M. Quack, *Energy Redistribution in Reacting Systems, chapter A.3.13 in Encyclopedia of Chemical Physics and Physical Chemistry*, J. H. Moore, N. Spencer (Eds), pp. 897–936, IOP publishing, Bristol, **2001**.
[110] M. Quack, *Chimia* **2003**, *57*, 147–160.
[111] A. Kushnarenko, E. Miloglyadov, M. Quack, G. Seyfang, *Phys. Chem. Chem. Phys.* **2018**, *20*, 10949–10959.

[112] M. Hippler, M. Quack, R. Schwarz, G. Seyfang, S. Matt, T. Märk, *Chem. Phys. Lett.* **1997**, *278*, 111–120.
[113] H. Schwarz, K. R. Asmis, *Chem. Eur. J.* **2019**, *25*, 2112–2126.
[114] P. R. Shirhatti, I. Rahinov, K. Golibrzuch, J. Werdecker, J. Geweke, J. Altschäffel, S. Kumar, D. J. Auerbach, C. Bartels, A. M. Wodtke, *Nat. Chem.* **2018**, *10*, 592–598.
[115] M. T. Cvitas, J. O. Richardson, *Quantum Dynamics in Water Clusters, Chapter 9 in Molecular Spectroscopy and Quantum Dynamics*, R. Marquardt, M. Quack (Eds), pp 301–326, Elsevier, Amsterdam, **2021**.
[116] F. Bergasa-Caceres, E. Haas, H. A. Rabitz, *J. Phys. Chem. B* **2019**, *123*, 4463–4476.
[117] P. Faccioli, M. Sega, F. Pederiva, H. Orland, *Phys. Rev. Lett.* **2006**, *97*, 108101.
[118] S. a Beccara, L. Fant, P. Faccioli, *Phys. Rev. Lett.* **2015**, *114*, 098103.
[119] C. Micheletti, P. Hauke, P. Faccioli, *Phys. Rev. Lett.* **2021**, *127*, 080501.
[120] R. G. Weiß, M.-E. Losfeld, M. Aebi, S. Riniker, *J. Phys. Chem. B* **2021**, *125*, 9467–9479.

Manuscript received: June 15, 2023
Revised manuscript received: July 6, 2023
Version of record online: July 31, 2023